Elsevier Editorial System(tm) for Ceramics International

Manuscript Draft

Manuscript Number: CERI-D-19-04816R1

Title: Mg/Cu co-substituted hydroxyapatite - biocompatibility, mechanical properties and antimicrobial activity

Article Type: Full length article

Keywords: A. Sintering; C. Mechanical properties; E. Biomedical application; Hydroxyapatite

Corresponding Author: Dr. Djordje N Veljovic, Ph.D.

Corresponding Author's Institution:

First Author: Djordje N Veljovic, Ph.D.

Order of Authors: Djordje N Veljovic, Ph.D.; Tamara Matic; Tanja Stamenic; Vesna Kojic; Suzana Dimitrijevic-Brankovic; Miodrag J Lukic; Sanja Jevtic; Zeljko Radovanovic; Rada Petrovic; Djordje Janackovic

Abstract: The aim of this study was to improve the mechanical properties and to optimize antimicrobial activity of hydroxyapatite (HAP) by simultaneous doping with Mg and Cu ions in order to obtain material that would be able to assist in the bone/tooth healing process, prevent post-implementation infections and provide satisfying values of hardness and fracture toughness for biomedical application. Ion doping was done during the hydrothermal synthesis of HAP powders, whereby the content of Mg ions in the starting solution was varied between 1-20 mol. % with regard to Ca ions, while the amount of Cu ions was kept constant at 0.4 mol. %. The green compacts were sintered for 2 h at temperatures ranging 750-1200 °C depending on the Mg content, chosen in agreement with dilatometry results. Presence of Mg ions was found to favour transition from HAP to □□tricalcium phosphate phase (□□TCP□, which enabled formation of biphasic HAP/□□TCP and pure □□TCP phase at 160 °C during hydrothermal synthesis. In vitro investigation of antimicrobial activity against Escherichia coli, Staphylococcus aureus and Enterococcus faecalis showed satisfactory antimicrobial activity. MTT assay performed on MRC-5 and L929 cell lines showed excellent cytocompatibility and cell proliferation. Maximum hardness by Vickers and fracture toughness values, 4.96 GPa and 1.75 MPa m1/2 respectively, were obtained upon addition of 5 mol. % Mg, as a consequence of the lowest grain size and porosity, as well as the highest densification rate. This is, to the best of our knowledge, the highest fracture toughness for HAP or □-TCP ceramics reported thus far.

Mg/Cu co-substituted hydroxyapatite – biocompatibility, mechanical properties and antimicrobial activity

Djordje Veljovic[1], Tamara Matic[2], Tanja Stamenic[1], Vesna Kojic[3], Suzana Dimitrijevic-Brankovic[1], Miodrag J. Lukic[4], Sanja Jevtic[1], Zeljko Radovanovic[2], Rada Petrovic[1], Djordje Janackovic[1]

[1] University of Belgrade, Faculty of Technology and Metallurgy, Karnegijeva 4, Belgrade 11120, Serbia

[2] University of Belgrade, Innovation Center of Faculty of Technology and Metallurgy, Karnegijeva 4, Belgrade 11120, Serbia

[3] University of Novi Sad, Faculty of Medicine, Oncology Institute of Vojvodina, Put Dr Goldmana 4, 21204 Sremska Kamenica, Serbia

[4] University of Belgrade, Institute of Technical Sciences of the Serbian Academy of Sciences and Arts, Knez Mihailova 35/IV, 11000 Belgrade, Serbia

Correspondence to: Djordje Veljovic; e-mail: djveljovic@tmf.bg.ac.rs, phone: +38111-3303720, fax: +38111-3370387

Abstract

The aim of this study was to improve the mechanical properties and to optimize antimicrobial activity of hydroxyapatite (HAP) by simultaneous doping with Mg and Cu ions in order to obtain material that would be able to assist in the bone/tooth healing process, prevent post-implementation infections and provide satisfying values of hardness and fracture toughness for biomedical application. Ion doping was done during

the hydrothermal synthesis of HAP powders, whereby the content of Mg ions in the starting solution was varied between 1-20 mol. % with regard to Ca ions, while the amount of Cu ions was kept constant at 0.4 mol. %. The green compacts were sintered for 2 h at temperatures ranging 750-1200 °C depending on the Mg content, chosen in agreement with dilatometry results. Presence of Mg ions was found to favour transition from HAP to β–tricalcium phosphate phase (β–TCP), which enabled formation of biphasic HAP/β–TCP and pure β–TCP phase at 160 °C during hydrothermal synthesis. *In vitro* investigation of antimicrobial activity against *Escherichia coli*, *Staphylococcus aureus and Enterococcus faecalis* showed satisfactory antimicrobial activity. MTT assay performed on MRC-5 and L929 cell lines showed excellent cytocompatibility and cell proliferation. Maximum hardness by Vickers and fracture toughness values, 4.96 GPa and 1.75 MPa $m^{1/2}$ respectively, were obtained upon addition of 5 mol. % Mg, as a consequence of the lowest grain size and porosity, as well as the highest densification rate. This is, to the best of our knowledge, the highest fracture toughness for HAP or β-TCP ceramics reported thus far.

Keywords: A. Sintering; C. Mechanical properties; E. Biomedical application; Hydroxyapatite;

1. Introduction

Calcium hydroxyapatite (HAP) is widely investigated biomaterial due to its chemical and structural similarity with the mineral constituent of human bone and teeth. In addition, HAP possesses desired properties such as bioactivity, biocompatibility, osteoconductivity, osteoinductivity as well as ability to stimulate osseointegration [1]. Owing to this, it has found wide applications: as an implant material and metallic

prostheses coating in maxillofacial, dental and orthopaedic surgery [2-6], in drug-, gene- or protein- carrier delivery systems [7-9], as a bone graft material and particulate filler for bone defects [10] and material for dental fillings and periodontal treatments [1]. However, compared to the human bone mineral, synthetic HAP has inferior mechanical properties.

Biological HAP usually contains a large variety of trace elements such as: Mg, F, Si, Sr, Zn etc. By introducing these elements into the HAP structure during synthesis process, one may mimic the mineralization of biological HAP and thus regulate the phase composition and morphology, as well as produce biomaterial with improved biological and mechanical properties [11].

Magnesium is one of the dominant substitutes for calcium in the bone mineral due to their chemical similarity. Magnesium ions are known to promote bone mineralization and osteoblast-like cell proliferation, thus enhancing bioactivity and biocompatibility of material [12]. Bone fillers based on HAP doped with Mg ions have been reported to improve the interaction between the implant material and human osteoblast and mesenchymal stem cells, as well as formation of the new bone tested *in vitro* and *in vivo* [13,14]. Substitution of the Ca ion with smaller ion, such as Mg, rises strain in the lattice which favours the HAP-β–TCP transition and may result in the formation of biphasic calcium phosphates (BCP) [15-17]. BCP, a mixture of stable HAP and highly resorbable β–TCP, due to its specific dissolution characteristics has ability to intensely promote new bone formation at the implant site [2,18].

Frequent post-implementation infections, usually associated with implant materials, led to new research approach in metal ion-doping for antimicrobial activity of

biomaterials. Metal ions such as Cu^{2+}, Zn^{2+}, Ag^{+} are well known antimicrobial agents, however, if present in high doses they are shown to be cytotoxic [19-22]. Copper is an essential trace element in human body. Besides its bactericidal effect, it has a role in the cross-linking of collagen and bone elastin [23,24]. Previously reported study [20] investigated effects of different concentrations of Cu ions in the HAP structure on its antimicrobial activity and cytotoxicity, and it was concluded that doping of HAP with 0.4 mol. % of Cu ions provided high antimicrobial properties, but lowered the biocompatibility of the HAP-based material. In this study, the aim was to keep aforementioned concentration of Cu ions in order to provide high antimicrobial properties, while compensating for the decrease in biocompatibility with addition of Mg ions.

The aim of this study was to improve mechanical and antimicrobial properties of synthetic HAP by simultaneous ion doping with Mg and Cu in order to obtain bioactive material that would be able to 1) assist in the bone/tooth healing process; 2) prevent post-implementation infections; 3) provide satisfying values of hardness and fracture toughness. To the best of our knowledge this was the first time that Cu and Mg ions were simultaneously used as dopants in HAP in bioceramic, with varying the Mg content. Mg,Cu-HAP could potentially be used both in the compact form and in the form of calcinated powder for diverse applications in orthopaedic, maxillofacial and dental surgery, regenerative medicine and tissue engineering. Mg,Cu-HAP could also find application as a restorative dental material (i.e. bioactive dental insert [25], bioactive composite filler [26]). The effects of doped ions on the mechanical properties, biocompatibility, antimicrobial activity and sintering behaviour were also investigated.

2. Materials and methods

2.1. Mg,Cu- doped hydroxyapatite powder synthesis

Eight different nanosized calcium-hydroxyapatite based powders were synthesized in this study by a previously described modified hydrothermal method [27-29]. Precursor solution of the control sample (pure HAP, c-HAP in Table 1) consisted of $Ca(NO_3)_2 \cdot 4H_2O$, $Na_2H_2EDTA \cdot 2H_2O$, $NaH_2PO_4 \cdot 2H_2O$ and urea. Substitution of Ca ions with Mg and Cu in the Mg,Cu-doped HAP samples was performed during hydrothermal synthesis by introducing Mg and Cu ions in the precursor solution. As Mg and Cu ions sources, $Mg(NO_3)_2 \cdot 6H_2O$ and $Cu(NO_3)_2 \cdot 3H_2O$ were used. The content of Mg ions in the precursor solution varied between 1-20 mol. % with regard to Ca ions amount. The concentration of Cu ions was kept constant at 0.4 mol. % related to the concentration of Ca ions in all doped samples. The composition of starting solutions for each sample is shown in the Table 1. The Ca+Mg+Cu/P ratio value for all samples was 1.67. The precursor solutions were thermally treated in autoclave at 160 °C for 3 hours, under p = 8 bar. The obtained precipitates were collected by vacuum filtration, flushed with deionized (DI) water and dried at 105 °C.

Table 1. *The composition of precursor solutions for hydrothermal synthesis of each sample*

2.2. Characterization of sample powders

2.2.1. X-ray Diffraction Analysis

Phase identification of the samples before and after sintering was determined by X-ray diffraction (XRD), conducted on X-ray diffractometer (Ital Structure APD 2000) with CuKα radiation (1.54 Å) in the 2θ angle ranging from 10° to 65° with a scan step

of 0.02° s^{-1}. Crystallographic identification of the phases was accomplished by comparing the experimental XRD patterns with standards compiled by the Joint Committee on Powder Diffraction Standards cards, JCPDS 09-0169, JCPDS 09-0348 and JCPDS 09-0432 for β–TCP, α–TCP and HAP respectively.

2.2.2. Scanning electron microscopy and energy dispersive X-ray analysis

A scanning electron microscope (Tescan FE-SEM Mira 3 XMU) operated at 20 keV was employed to characterize the morphology of the powders. All samples were coated with gold/palladium alloy using a sputter coater (Polaron SC503, Fisons Instruments) prior to SEM analysis. In order to confirm incorporation of Cu and Mg ions in all samples, energy dispersive X-ray (EDX) analysis was performed on Oxford Inca 3.2 coupled with SEM Jeol JSM 5800, operated at 20 keV. The results of EDX analysis are presented as average arithmetical value of three measurements of different surface areas of the sample at the 1000 times magnification, expressed in atomic percentages.

2.2.3. TGA/DTA analysis

In order to determine thermal behaviour of the samples, a simultaneus thermogravimetric and differential thermal analysis (TG/DTA) was performed in alumina crucibles (Setsys Evolution, Setaram). TG/DTA measurements were performed in air, with heating/cooling rate of 20 °C/min, from room temperature to 1200 °C.

2.2.4. In vitro biocompatibility of Mg,Cu-HAP powders

The biocompatibility of the Mg,Cu-HAP powder samples was tested by measuring cell viability using the MTT assay on two different fibroblast cell lines: L929 and MRC-5. The L929 line was of a mouse origin, whereas the MRC-5 was a human

fibroblast cell line. MTT assay was performed by following previously reported procedure [3], using 96-well culture plates (ICN, Costa Mesa, CA) (0.5 x 10^4 cells/well). The number of replicates was six. The optical density (OD) of the developed colour was read at 570/650 nm (Behring ELISA Processor II) after 24, 48, 72 and 96 h, and the results were presented as a relative cell viability compared to the OD of the control cells taken as 100 %. The viability of cells used in the experiment was greater than 90 %. The agar diffusion test (ADT) was performed according to international standards (ISO 10993-5, ISO7405) following previously reported procedure [3].

2.2.5. Antimicrobial activity of Mg,Cu-HAP powders

Antimicrobial activity was determined by microbial inhibition test using three indicator cultures: *Escherichia coli* (ATCC 25922), *Staphylococcus aureus* (ATCC 25922), and *Enterococcus faecalis* (ATCC 29212). The inoculums of all microorganisms were prepared from fresh overnight broth cultures (Tripton soy broth + 0.6% yeast extract, Torlak, Belgrade) that were incubated at 37 °C. Each powder sample of 0.1 g weight was placed in a test tube, followed by addition of 0.9 cm^3 of sterile saline and 0.1 cm^3 of diluted culture (cca 10^5 cell per ml). After 2 hours of incubation at 37 °C, additional 9 cm^3 of sterile saline was added to every tube. Aliquots of 0.1 cm^3 were then taken from each tube placed in the sterile Petri dishes and covered with Tryptone Soya Agar (TSA). After solidification of TSA, the Petri dishes were incubated for 24 h at 37 °C. The formed bacterial colonies were counted and the degree of inhibition (R) was calculated following the equation:

$$R = [(C_0\text{-}C)/C_0\ ] \text{ x } 100\ [\%] \qquad (1)$$

where C_0 is the concentration of culture in the control; C is the concentration of culture in powder sample. All samples were treated in triplicate and the results are expressed as the mean value.

2.3. Processing of Mg,Cu-doped hydroxyapatite green compacts

The Mg,Cu-doped hydroxyapatite powders were uniaxially pressed into green compacts at 300 MPa (CIP-15, MTI Corporation) during 1 min, using a high-quality cylindrical steel mould with diameter of 8 mm.

2.4. Dilatometric analysis

Sintering behaviour of the samples was investigated by a vertical dilatometer (Setsys Evolution, Setaram). Samples c-HAP, HAP0, HAP1, HAP5 and HAP7.5 were heated up to 1200 °C, while HAP10, HAP15 and HAP20 were heated up to 1100 °C, with the same heating/cooling rate value of 20 °C/min. All samples had initial diameter of 8 mm.

2.5. Sintering of Mg,Cu-doped hydroxyapatite compacts

Based on results of TGA/DTA and dilatometric analysis of Mg,Cu-doped HAP powders as well as SEM micrographs of the samples after dilatometric analysis, optimal sintering temperature for each sample was chosen: 1200 °C for samples with lower Mg content (up to 7.5 mol. %), 1000 °C for HAP10 and 750 °C for HAP15 and HAP20 samples. The green compacts were sintered in high-temperature furnace for 2 h at the heating rate of 20 °C/min. Upon sintering, all samples were naturally cooled down to the room temperature.

2.6. Characterization of sintered samples

2.6.1. Microstructure and mean grain size determination of Mg,Cu-HAP sintered compacts

Microstructures of sintered materials were determined by using FE-SEM, applying the same scanning conditions as aforementioned. Average grain sizes (AGS) of the compacts were determined from the micrographs of the polished and thermally etched surface. The total number of 100 grains was used in order to calculate AGS.

2.6.2. Density and relative linear shrinkage of Mg,Cu-HAP sintered compacts

The density of obtained samples was determined by using Archimedes' principles, while relatively linear shrinkage (*RLS*) was determined by the equation:

$$RLS = (d_0\text{-}d)/d_0 \quad (2)$$

where d_0 is an initial diameter and d is a diameter of the compact after sintering.

2.6.3. Mechanical properties of Mg,Cu-HAP sintered compacts

The Vickers hardness (*HV*) and fracture toughness (K_{IC}) of polished sintered samples were measured by applying 1.0 kg load with a dwell time of 5 s on a Vickers Hardness Indentation Tester (Buehler Indentament 1100 series). *HV* was calculated by the equation (3) based on the diagonal dimension of prints on the obtained samples, while K_{IC} of polished sintered samples was determined using the Evans and Charles equation (4):

$$HV = 1854.4 \cdot X \cdot (0.168 \cdot N)^{-2} \text{ [GPa]} \quad (3)$$

where X is load mass [g], N is dimension of the diagonal print [μm]

$$K_{IC} = 0.0824 \cdot P \cdot c^{-3/2} \text{ [MPa/m}^{1/2}\text{]} \quad (4)$$

where P is the identation load [N], c is length of the induced radial crack [μm]

Hardness by Vickers (HV) and fracture toughness (K_{IC}) values were presented as an average arithmetical value for five measurements per sample. The mean value and standard deviation were calculated using Origin Pro software (OriginLab Corporation). The one-way analysis of variance (ANOVA) and Tukey post-hoc test were used to evaluate the significant difference among samples with the level of significance set at 0.05.

3. Results and discussion

3.1. Characterization of the sample powders

3.1.1. XRD and EDX analysis

The XRD diffractograms of the Mg,Cu-HAP powder samples are shown in the Fig. 1. The XRD patterns of HAP1 and HAP5 show only peaks characteristic of apatite phase, as seen in the case of c-HAP and HAP0 (0 mol.% Mg, 0.4 mol. % Cu) samples reported in the previous study [20]. In the case of HAP7.5 and HAP10, apatite phase partly transformed into β–TCP and its relative intensity increased with increasing the Mg ion content. Presence of Mg ions in the starting solution inhibits apatite crystallization and favours its thermal conversion into β–TCP phase. This finding is in good agreement with the literature data [16,17,30]. The powders HAP7.5 and HAP10 were biphasic BCP powders with dominant β–TCP phase. However, when more than 15 mol. % of Ca ions was substituted with Mg ions in the precursor solution, apatite phase was completely absent and monophasic β–TCP powders were formed.

Fig. 1. *XRD patterns of the as-prepared powder samples*

Similar results were reported in studies by *Fadeev et al.* and *Ren et al.* where addition of Mg ions above 10 at. % [17] and at 20 mol. % [31] led to pure Mg substituted *β*–TCP powder. According to *Fadeev et al.*, the destabilizing effect of magnesium on HAP lattice is attributed to the smaller ionic radius of Mg^{2+} (0.65 Å) in comparison with that of Ca^{2+} (0.99 Å). Substitution of the smaller ion in the HAP lattice rises strain in the lattice, which favours the HAP-*β*–TCP transition [17].

The results of the EDX analysis of the Mg,Cu-HAP powders are shown in the Table 2. The presence of Mg ions as dopant in all the samples was confirmed, while concentrations of Cu ions were within the determination limit. The Ca/P and (Ca+Mg+Cu)/P ratios in all doped samples were less than the stoichiometric ratio of the hydroxyapatite (1.67).

Table 2. *Elemental composition of the obtained powders*

In general, the Mg content in the products increased upon increasing the amount of Mg source in the precursor solution. The maximum content of Mg ions incorporated in the HAP structure was 1.35 at. % in the sample HAP20, which is approximately 10.6 mol. % in relation to calcium.

3.1.2. SEM analysis

The SEM micrographs of the Mg,Cu-HAP as-synthesised powders (Fig. 2) show that all powders were composed of relatively uniform spherical agglomerates, ranging in size from few hundred nm to several microns. The size of the agglomerates did not significantly vary regardless of the amount of Mg ions present in the structure. In the case of HAP1 the spherical particles were composed of nano-rods (Fig. 2.a), while in

the case of HAP5 the nano-rods were noticeably rounder and more densely packed (Fig. 2.b). Upon increasing the Mg content in the starting solution, the roundness of the sub-particles and their packing density in the obtained powders tended to increase as well, resulting in cauliflower-like agglomerates (Fig. 2.d-f).

Fig. 2. *SEM micrographs of the obtained powders: a)HAP1; b)HAP5; c)HAP7.5; d)HAP10; e)HAP15; f)HAP20*

3.1.3. Antimicrobial activity

The results of antimicrobial activity of the as-prepared powder samples against three cultures: *E. coli*, *S. aureus*, and *E. faecalis* are shown in the Table 3. In literature [32,33] it was found that pure HAP showed some cell reduction compared to the blank during antimicrobial tests, thus in this work the degree of reduction (*R* (%)) was calculated in relation to the pure HAP, in order to show only the effect of the doped ions. Most samples were more effective against *E.coli* and *S.aureus*, compared to *E.faecalis*. In the case of *S.aureus* there was a clear rise in the inhibition rate upon adding more than 10 mol. % of Mg ions. In contrast, in the case of *E.faecalis* higher degree of inhibition was observed when content of Ca ions substituted by Mg was kept below 10 mol. %.

The antibacterial activity of the hydroxyapatites doped with metal ions is well documented [34-36]. There are few proposed bactericidal mechanisms of metal ions that cause different types of injuries to microbial cells as a result of oxidative stress, protein dysfunction or membrane damage [37]. Cu ions have an ability to generate reactive oxygen species (ROSs) that induce oxidative stress within the cell [34]. Gram negative *E. coli* and gram positive *E. faecalis* are considered as susceptible to Cu ions [38,39].

However, some bacteria, such as *S. aureus* expresses the mechanisms protecting them from the toxic effect of the copper induced ROSs activity [40].

On the other hand, Mg ions exhibit also non-oxidative mechanisms of bactericidal activity such as pH increasing in water around the ion surface [41,42]. This phenomenon can explain the slight bactericidal effect of the sample HAP0 tested on *S. aureus* strain (Table 3), with Cu and without Mg ions. However, with increasing of the Mg content, the cell death rate of *S. aureus* also increased, and it reached 97.67 % in HAP20. On the contrary, the increase of the Mg content, decreases the inhibition capacity of the HAP samples for *E. faecalis* strain, since the Cu content decreases. The lowest inhibition of *E. faecalis* is achieved with the HAP20, where the Cu content decreased (Tables 2 and 3) probably due to low susceptibility to Mg ions and evident alkaline resistance [43]. A slight decrease of HAPs inhibitory activity on *E. coli* with the Mg content increase can also be noted, but it is not sufficient for explanation of the possible dominant mechanism(s) of action.

The overall results of our research demonstrated that all the samples have higher ability than pure HAP to reduce number of colonies of *E. coli*, *E. faecalis* and *S.aureus* and thus may prevent infections at the implementation site.

Table 3. *Results of antibacterial activity of the samples*

3.1.4. In vitro biocompatibility of Mg,Cu-HAP powders

In order to test biocompatibility of the as-prepared powders, *in vitro* agar diffusion and MTT assays were commenced. The results of the agar diffusion assay showed that the lysis index in all the cases was zero, i.e. the Mg,Cu-HAP samples were not cytotoxic towards MRC-5 and L929 cell lines, as no detectable discoloration or any difference in

staining intensity around or under the Mg,Cu-HAP samples was observed. The MTT assay results of MRC-5 and L929 cell lines are shown in the Fig. 3. The number of cells increased over time in the evaluated period in all cases. As expected, addition of Cu ions lowered the mean cell viability of both cultures compared to the pure HAP. In contrast, it has been proved in this study that the presence of Mg ions stimulates cell proliferation and improves biocompatibility. This may be explained by different phase composition of the samples, different shape of particles, as well as different solubility between HAP and β–TCP phases, which impacts the level of dopant ion released etc. [44]. According to the literature data, doping HAP, β–TCP and BCP with Mg ions increases cell viability and promotes osseointegration [13,14,30,45,46]. *Liangzhi et al.* reported that incorporation of Mg ions in the HAP lattice increases cell proliferation compared to the pure HAP, with an increasing trend up to 10 mol. % of Mg ions [47].

In the present study, in the case of MRC-5 cell line, the cells in contact with HAP15 sample exhibited the best results, while in case of L929 cell line, the best promotion effect was found in HAP7.5 and HAP10 samples. By comparing the mean values of the cell viability, it may be concluded that the cell proliferation of Mg,Cu-HAP samples was higher on MRC-5 culture, a human fibroblast cell line, compared to L929 which is of a mouse origin. Finally, it can be concluded that the prepared samples have a great cytocompatibility and an excellent ability to promote cell adhesion and spreading, which make them suitable for use in biomedical application.

Fig. 3. *Results of the MTT assay performed on: a) MRC-5; b) L929 cell line*

3.1.5. TGA/DTA and dilatometric analysis

According to the TGA curves (Fig. 4.a), the mass loss of all the powders was relatively small during heating up to 1200 °C and amounted to approximately 6-7 wt. %. The weight loss up to 200 °C was most likely caused by the elimination of physically adsorbed water and CO_2, which can be seen as an endothermic peak on the DTA curves [31,48]. In the case of the c-HAP, HAP0, HAP1 and HAP5 samples, the abrupt weight loss around 800-900 °C region could be observed, which is probably due to the loss of H_2O during phase transition from HAP to *β*–TCP phase [31]. This is in good agreement with the exothermic peak around 800 °C on the DTA curves of the samples with Mg content up to 7.5 mol. %. The powders with Mg content of 10 mol. % and higher had a low amount (HAP10) or complete absence (HAP15, HAP20) of HAP phase in the structure. Therefore, HAP-*β*–TCP phase transition did not take place, which was manifested as a lack of mass loss and characteristic exothermic peak in 800-900 °C region on the TGA and DTA curves.

Fig. 4. *a) TGA and b) DTA curves of the samples*

The dilatometric curves of all the samples are compared in the Fig. 5. The shrinkage progressed continuously with the exception of the sample HAP20, which begun to intensely shrink below 800 °C. The samples containing high Mg content (10 mol. % and above) manifested a sudden expansion at the temperatures above 1100 °C on the dilatometric curve, which is associated with swelling and melting start point. In order to avoid region of the thermal expansion, the following sintering temperatures were chosen: 1200 °C for c-HAP, HAP0, HAP1, HAP5 and HAP7.5, 1000 °C for HAP10 and 750 °C for HAP15 and HAP20 samples.

Fig. 5. *Dilatometric curves*

3.2. Characterization of the sintered samples

3.2.1. XRD analysis

The XRD patterns of the Mg,Cu-HAP sintered samples and the control sample (c-HAP, 0 % Cu, 0 % Mg) sintered at 1200 °C are shown in the Fig. 6. The sintering temperature was 1200 °C for samples with Mg content up to 7.5 mol. %, 1000 °C for HAP10 and 750 °C for HAP15 and HAP20 samples. Calcium-hydroxyapatite undergoes phase transition into β–TCP when heated above 800 °C, and if heated further, it transforms into α–TCP phase at 1125 °C [1,49,50]. The XRD pattern of c-HAP sintered at 1200 °C shows that apatite phase was dominant in the structure. As expected, a high amount of HAP underwent phase transition into α–TCP, and only traces of β–TCP phase could be found. The β–α transition is not desirable due to its effect on lowering mechanical properties of HAP based material and can be avoided by stabilizing β–TCP phase [51]. It was previously reported that the presence of Mg ions in HAP structure has ability to stabilize β–TCP phase by increasing the β–α transformation temperature [16,30,49], that was also confirmed in this study. Upon substitution of 1 mol. % of Ca ions with Mg ions, the amount of α–TCP present in the structure was significantly lowered in favour of β–TCP phase. The XRD patterns of HAP5 suggest that substitution of 5 mol. % of Ca ions with Mg ions led to complete absence of β–α transition up to 1200 °C, resulting in the biphasic structure (BCP) with equally dominant HAP and β–TCP phases. This structure may be desired feature for a biomedical application as BCPs have a good bioactivity owing to the high solubility of β–TCP phase, but unlike β–TCP ceramics, they are stable during the bone ingrowth process due to the presence of HAP [52]. As β–TCP is more resorbable than HAP, the

BCP-based implants also have rough surface, which provides high interfacial strength between the bone and the implant [30]. The XRD diffractograms of the samples HAP7.5-HAP20 indicate that substitution of more than 7.5 mol. % of Ca ions with Mg ions led to the complete phase transition of apatite phase into *β*–TCP after sintering.

Fig. 6. *XRD patterns of the sintered samples: c-HAP-HAP7.5 (1200 °C); HAP10 (1000 °C); HAP15, HAP20 (750 °C)*

3.2.2. SEM analysis

Effects of the dopants on the samples' microstructure were monitored engaging FE-SEM upon sintering (Fig. 7), and glaring discrepancy in the microstructures may be observed. The amount and the size of pores noticed in the sintered compacts are affected by many reasons: (i) the morphology of the HAP powder sub-particles and spherical agglomerates, (ii) the presence of harder or softer agglomerates and (iii) more or less intensive phase transformation of HAP to *β*–TCP. All of the aforementioned causes are strongly affected by the presence of the Mg ions, and vary according to its content. The amount of the pores was reported to increase with the Mg content ranging between 0.6 to 2.4 wt. % in the case of HAP produced by the precipitation method [16]. In this study, addition of Mg up to 5 mol. % led to decrease in overall porosity. However, when more than 7.5 mol. % of Mg was added, densification process was inhibited and porosity steadily increased resulting in highly porous structure of HAP10, HAP15 and HAP20 samples, most likely caused by the incomplete densification process.

Table 4. *Density and relative linear shrinkage of the sintered samples*

The relative linear shrinkage (*RLS*) can be associated to the densification process. In the literature data it is evidenced that incorporation of Mg ions into the HAP structure gains density of the HAP based ceramics [36,53]. In this study, the incorporation of Mg ions led to a higher densification of the HAP (HAP1) and BCP based (HAP5) ceramics, i.e. higher *RLS* values and higher fire densities (Table 4). The addition of 5 mol. % of Mg ions led to the highest densification upon sintering at 1200 °C (*RLS*=17.50 %, ρ=3.01 g/cm^3). Due to the high porosity of the samples with the Mg content more than 10 mol. %, relative linear shrinkage (*RLS*) and density values of those samples were not calculated.

The FE-SEM micrographs of the polished and thermally etched samples HAP0, HAP1 and HAP5 used for calculating average grain size are shown in the Fig. 8. The samples c-HAP and HAP0 did not significantly differ with the average pore size of approximately 1 μm, which is in good agreement with the literature [54]. On the other hand, variation of the Mg content had a great impact on the porosity. The addition of 1 mol. % Mg led to overall decrease in porosity and to more spherically shaped pores, with no influence on average grain size (Fig. 8.b). In the case of HAP5 sample, a material with lowest porosity and small average grain size (0.50 μm) was obtained (Fig. 8.c). A decrease in the grain size could potentially lead to increase in the fracture toughness and hardness values, as it did in the case of recent investigation [3,54].

Fig. 7. *Microstructure of the Mg,Cu-HAP sintered samples: a)HAP0 (1200 °C); b)HAP1 (1200 °C); c)HAP5 (1200 °C); d)HAP7.5 (1200 °C); e)HAP10 (1000 °C); f)HAP15 (750 °C); g)HAP20 (750 °C)*

Fig. 8. *SEM micrographs of etched samples sintered at 1200 °C: a) HAP0; b) HAP1; c) HAP5*

3.2.3. Mechanical properties

The hardness by Vickers (*HV*) and the fracture toughness (K_{IC}) values shown in Fig. 9 and Fig. 10 respectively present average arithmetical values for five measurements per sample. The mechanical properties of HAP or BCP based materials reported so far ranged from 2.7 to 6.1 GPa (*HV*) and from 0.9 to 1.58 MPa·m $^{1/2}$ (K_{IC}) [15,54-60]. However, the aforementioned results were obtained under different measuring and processing conditions (lower loads applied during mechanical test or higher pressure applied during material processing), thus cannot be easily compared. For instance, sintered compacts of the undoped HAP and HAP doped with 0.4 mol. % of Cu previously reported [54] manifested higher *HV* and lower K_{IC} values (*HV*= 3.71 and 3.85 GPa; K_{IC}= 1.19 and 1.46 MPa· $m^{1/2}$ of pure HAP and Cu-HAP respectively) compared to c-HAP and HAP0 samples obtained in the present study, even though the synthesis method, Cu content and sintering conditions were identical. Lower hardness values can easily be explained by the lower pressure applied during isostatic pressing in this study (300 MPa instead of 400 MPa), which led to more spherically shaped pores and slightly higher overall porosity. As previously described [61], spherical pores induce an increase in the fracture toughness of the sintered HAP biomaterials, which explains higher K_{IC} values obtained in this study compared to the previously reported values [54].

Fig. 9. *Hardness by Vickers of the sintered Mg,Cu-HAP samples*

Fig. 10. *Fracture toughness of the sintered Mg,Cu-HAP samples*

That being said, remarkably high *HV* values, 4.12 and 4.96 GPa, have been obtained in the case of HAP1 and HAP5 samples respectively. Substitution of 1 and 5 mol. % of Ca ions with Mg ions significantly ($p < 0.05$) increased *HV* values by 54.3 % and 85.8

% respectively, in comparison to the undoped HAP sample. The addition of 5 mol. % of Mg ions extremely improved fracture toughness of HAP, with an average value of 1.75 MPa·$m^{1/2}$, which is, to the best of our knowledge, the highest K_{IC} value for the HAP or BCP material reported so far. The increase in the mean *HV* and K_{IC} values of the HAP5 sample may be attributed to the dense structure with low porosity and small grain size, as grain boundaries make major contribution to cracking resistance [1]. Similar trend was reported by *Ryu et al.* [30]. The extraordinary hardness and fracture toughness of HAP5 material make it promising for biomedical application. In the case of human dentin, the fracture toughness was found to be in the range of 1.13-2.02 MPa· $m^{1/2}$, which indicates that HAP5 could be also used as a dentin substitute. The mean *HV* and K_{IC} values had tendency to decrease with ≥ 7.5 mol. % Mg content in the structure, which is in accordance with their highly porous microstructure.

4. Conclusion

The present study investigated effects of the simultaneous Cu, Mg ion doping of HAP obtained by hydrothermal synthesis on its biological and mechanical properties. The Mg content was varied between 1-20 mol. %, while the Cu content was kept constant at 0.4 mol. % with regard to Ca ions amount.

- With the addition of Mg, the rod-like HAP sub-particles obtained more spherical shape, resulting in cauliflower-like agglomerates.
- Presence of Mg ions was found to favour HAP-β–TCP transition which enabled formation of BCP (7.5-10 mol.% Mg) and pure β–TCP phase at 160 °C (≥ 15 mol. % Mg).

- It was confirmed that Mg stabilizes β–TCP by suppressing β– to α–TCP phase transition. The addition of 0.4 mol. % Cu led to the overall good antimicrobial activity.
- The samples with content of Mg below 7.5 mol. % were more effective against *E.faecalis*, whilst the samples with Mg content above 7.5 mol. % manifested better antimicrobial properties against *S.aureus*. The results of antimicrobial tests in this research demonstrated that all samples reduced number of colonies of E. coli, E. faecalis and S.aureus and thus may prevent infections at the implementation site.
- All the Mg-containing samples showed excellent cytocompatibility and cell proliferation.
- The addition of Mg ions up to 5 mol. % led to a higher densification of the HAP and BCP based ceramics (HAP1 and HAP5), while addition of Mg ions above 7.5 mol. % resulted in highly porous structures with poor mechanical properties.
- The maximum hardness (4.96 GPa) and fracture toughness (1.75 MPa $m^{1/2}$) was obtained for HAP5 sample, which is, to the best of our knowledge, the highest fracture toughness for the HAP/BCP ceramics reported so far.
- Mg,Cu-HAP ceramics with the Mg content above 7.5 mol. % have monophasic β–TCP structure which is bioactive and soluble, cytocompatible and have good antimicrobial activity, which makes them appropriate for non-load-bearing biomedical application as osteoinductive, bioresorbable material with ability to prevent infections. Moreover, Mg,Cu-HAP powders with the Mg content above 15 mol. % synthesized in this study had a monophasic β–TCP structure, thus

may be used with no further heat treatment, which makes their use more energy- and cost-effective.

- Generally, HAP ceramics doped with Cu and Mg present osteoinductive biomaterials with satisfying values of hardness and fracture toughness, that are able to both assist in the bone healing process and prevent post-implementation infections, and could potentially be used both in the compact form and in the form of calcinated powder for diverse applications in orthopaedic, maxillofacial and dental surgery, regenerative medicine and tissue engineering.

Acknowledgments

The authors wish to acknowledge the financial support from the Ministry of Science and Technological Development of the Republic Serbia through the project III45019.

References

[1] S.V. Dorozhkin, Calcium orthophosphate bioceramics, Ceram. Int. 41 (2015) 13913–13966. https://doi.org/10.18321/ectj52.

[2] C.M. Kanno, R.L. Sanders, S.M. Flynn, G. Lessard, S.C. Myneni, Novel apatite-based sorbent for defluoridation: synthesis and sorption characteristics of nanomicrocrystalline Hydroxyapatite-Coated-Limestone, Environ. Sci. Technol. 48 (2014) 5798–5807. https://doi.org/10.1021/es405135r.

[3] Dj. Veljovic, M. Colic, V. Kojic, G. Bogdanovic, Z. Kojic, A. Banjac, E. Palcevskis, R. Petrovic, Dj. Janackovic. The effect of grain size on the biocompatibility, cell-

materials interface and mechanical properties of microwave-sintered bioceramics, J. Biomed. Mater. Res. A. 100 (2012) 3059–3070. https://doi.org/10.1002/jbm.a.34225.

[4] S. Dyshlovenko, C. Pierlot, L. Pawlowski, R. Tomaszek, P. Chagnon. Experimental design of plasma spraying and laser treatment of hydroxyapatite coatings. Surf. Coat. Tech. 201 (2006) 2054–2060. https://doi.org/10.1016/j.surfcoat.2006.04.055

[5] A. Fomin, S. Dorozhkin, M. Fomina, V. Koshuro, I. Rodionov, A. Zakharevich, N. Petrova, A. Skaptsov. Composition, structure and mechanical properties of the titanium surface after induction heat treatment followed by modification with hydroxyapatite nanoparticles. Ceram. Int. 42 (2016) 10838–10846. https://doi.org/10.1016/j.ceramint.2016.03.213

[6] A. Fomin, M. Fomina, V. Koshuro, I. Rodionov, A. Zakharevich, A. Skaptsov. Structure and mechanical properties of hydroxyapatite coatings produced on titanium using plasma spraying with induction preheating. Ceram. Int. 43 (2017) 11189–11196. https://doi.org/10.1016/j.ceramint.2017.05.168

[7] V. Uskokovic, T.A. Desai, Phase composition control of calcium phosphate nanoparticles for tunable drug delivery kinetics and treatment of osteomyelitis: I. Preparation and Drug Release. J. Biomed. Mat. Res. A 101 (2013) 1416–1426. https://doi.org/10.1002/jbm.a.34426.

[8] B. Mostaghaci, B. Loretz, C-M. Lehr, Calcium phosphate system for gene delivery: Historical background and emerging opportunities. Curr. Pharm. Des. 22 (2016) 1529–1533. https://doi.org/10.2174/1381612822666151210123859.

[9] M. Šupová, Substituted hydroxyapatites for biomedical applications: a review, Ceram. Int. 41 (2015) 9203–9231. https://doi.org/10.1016/j.ceramint.2015.03.316.

[10] S. Ghosh, V. Wu, S. Pernal, V. Uskokovic, Self-setting calcium phosphate cements with tunable antibiotic release rates for advanced bone graft applications, ACS Appl. Mater. Interfaces 8 (2016) 7691−7708. https://doi.org/10.1021/acsami.6b01160.

[11] C. Qi, Y-J Zhu, F. Chen, J. Wu, Porous microspheres of magnesium witlockite and amorphous calcium magnesium phosphate: microwave-assisted rapid synthesis using creatine phosphate, and application in drug delivery. J Mater. Chem. B 3 (2015) 7775−7786. https://doi.org/10.1039/c5tb01106j.

[12] C.M. Serre, M. Papillard, P. Chavassieux, J.C. Voegel, G. Boivin, Influence of magnesium substitution on a collagen-apatite biomaterial on the production of a calcifying matrix by human osteoblasts, J. Biomed. Mater. Res. 42 (1998) 626−633. https://doi.org/10.1002/(SICI)1097-4636(19981215)42:4<626::AID-JBM20>3.0.CO;2-S.

[13] E. Landi, A. Tampieri, M. Mattioli-Belmonte, G. Celotti, M. Sandri, A. Gigante, P. Fava, G. Biagini, Biomimetic Mg- and Mg, CO_3- substituted hydroxyapatites: synthesis

characterization and in vitro behaviour, J. Eur. Ceram. Soc. 26 (2006) 2593−2601. https://doi.org/10.1016/j.jeurceramsoc.2005.06.040.

[14] E. Landi, G. Logroscino, L. Proietti, A. Tampieri, M. Sandri, S. Sprio, Biomimetic Mg substituted hydroxyapatite: From synthesis to in vivo behaviour, J. Mater. Sci. Mater. Med. 19 (2008) 239−247. https://doi.org/10.1007/s10856-006-0032-y.

[15] S. Lala, T.N. Maity, M. Singha, K. Biswas, S.K. Pradhan, Effect of doping (Mg,Mn,Zn) on the microstructure and mechanical properties of spark plasma sintered hydroxyapatites synthesized by mechanical alloying, Ceram. Int. 43 (2017) 2389−2397. https://doi.org/10.1016/j.ceramint.2016.11.027.

[16] I. Cacciotti, A. Bianco, M. Lombardi, L. Montanaro, Mg-substituted hydroxyapatite nanopowders: Synthesis, thermal stability and sintering behaviour. J. Eur. Ceram. Soc. 29 (2009) 2969−2978. https://doi.org/10.1016/j.jeurceramsoc.2009.04.038.

[17] I.V. Fadeev, L.I. Shvorneva, S.M. Barinov, V.P. Orlovskii, Synthesis and structure of magnesium-substituted hydroxyapatite, Inorg. Mater. 39 (2003) 947−950. https://doi.org/10.1023/A:1025509305805.

[18] A. Gozalian, A. Behnamghader, M. Daliri, A. Moshkforoush, Synthesis and thermal behavior of Mg-doped calcium phosphate nanopowders via the sol gel method. Sci. Iran. F. 18 (2011) 1614−1622. https://doi.org/10.1016/j.scient.2011.11.014.

[19] O. Livitska, N. Strutynska, I. Zatovsky, I. Nikolenko, N. Slobodyanik, Y. Prylutskyy, M. Epple, O. Prymak, A. Byeda, Copper(II), zinc(II) and copper(II)/zinc(II)-containing carbonate-substituted hydroxyapatite: Synthesis, characterization and thermal behaviour, Mat.-wiss. u. Werkstofftech 47 (2016) 85−91. https://doi.org/10.1002/mawe.201600460.

[20] Z. Radovanovic, B. Jokic, Dj. Veljovic, S. Dimitrijevic, V. Kojic, R. Petrovic, Dj. Janackovic, Antimicrobial activity and biocompatibility of Ag^{+}- and Cu^{2+} -doped biphasic hydroxyapatite/-tricalcium phosphate obtained from hydrothermally synthesized Ag^{+}- and Cu^{2+}-doped hydroxyapatite, Appl. Surf. Sci. 307 (2014) 513−519. https://doi.org/10.1016/j.apsusc.2014.04.066.

[21] H.G. Petering, Pharmacology and toxicology of heavy metals: silver, Pharmacol. Ther. A 1 (1976) 127–130. https://doi.org/10.1016/0362-5478(76)90002-4.

[22] G. Borkow, J. Gabbay, Copper as a biocidal tool, Curr. Med. Chem. 12 (2005) 2163–2175. https://doi.org/10.2174/0929867054637617.

[23] C.D. Hunt, Copper and boron as examples of dietary trace elements important in bone development and disease, Curr. Opin. Orthop. 9 (1998) 28–36. https://doi.org/10.1097/00001433-199810000-00006.

[24] W. Opsahl, H. Zeronian, M. Ellison, D. Lewis, R.B. Rucker, R.S. Riggins, Role of copper in collagen cross-linking and its influence on selected mechanical properties of

chick bone and tendon, J. Nutr. 112 (1982) 708–716. https://doi.org/ 10.1093/jn/112.4.708.

[25] G. Ayoub G, Dj. Veljovic, M.L. Zebic, V. Miletic, E. Palcevskis, R. Petrovic, Dj. Janackovic, Composite nanostructured hydroxyapatite/yttrium stabilized zirconia dental inserts – The processing and application as dentin substitutes, Ceram. Int. 44 (2018) 18200–18208. https://doi.org/ 10.1016/j.ceramint.2018.07.028.

[26] T. Matic, M.L. Zebic, I. Cvijovic-Alagic, V. Miletic, R. Petrovic, Dj. Janackovic, Dj. Veljovic, The effect of calcinated hydroxyapatite and magnesium doped hydroxyapatite as fillers on the mechanical properties of a model BisGMA/TEGDMA dental composite initially and after aging, Metall. Mater. Eng. 24 (2018) 271–281. https://doi.org/10.30544/403.

[27] Dj. Janackovic, I. Petrovic-Prelevic, Lj. Kostic-Gvozdenovic, R. Petrovic, V. Jokanovic, D. Uskokovic, Influence of synthesis parameters on the particle sizes of nanostructured calciumhydroxyapatite. Key Eng. Mater 203 (2001) 192–195. https://doi.org/10.4028/www.scientific.net/KEM.192-195.203.

[28] Dj. Veljovic, E. Palcevskis, A. Dindune, S. Putic, I. Balac, R. Petrovic, Dj. Janackovic, Microwave sintering improves the mechanical properties of biphasic calcium phosphates from hydroxyapatite microspheres produced from hydrothermal processing, J. Mater. Sci. 45 (2010) 3175–3183. https://doi.org/10.1007/s10853-010-4324-8.

[29] B. Jokic, D. Radmilovic, D. Drmanic, S. Drmanic, R. Petrovic, Dj. Janackovic, Synthesis and characterization of monetite and hydroxyapatite whiskers obtained by a hydrothermal method, Ceram. Int. 37 (2011) 167–173. https://doi.org/10.1016/j.ceramint.2010.08.032.

[30] H.S. Ryu, K.S. Hong, J.K. Lee, D.J. Kim, J.H. Lee, B.S. Chang, D.H. Lee, C.K. Lee, S.S. Chung, Magnesia-doped HA/beta-TCP ceramics and evaluation of their biocompatibility, Biomaterials 25 (2004) 393–401. https://doi.org/10.1016/S0142-9612(03)00538-6.

[31] F. Ren, Y. Leng, R. Xin, X. Ge, Synthesis, characterization and ab initio simulation of magnesium-substituted hydroxyapatite. Acta Biomater. 6 (2010) 2787–2796. https://doi.org/10.1016/j.actbio.2009.12.044.

[32] Y. Li, J. Ho, C.P. Ooi, Antibacterial efficacy and cytotoxicity studies of copper(II) and titanium(IV) substituted hydroxyapatite nanoparticles, Mater. Sci. Eng. C 30 (2010) 1137–1144. https://doi.org/10.1016/j.msec.2010.06.011.

[33] V. Stanic, Dj. Janackovic, S. Dimitrijevic, S.B. Tanaskovic, M. Mitric, M.S. Pavlovic, A. Krstic, D. Jovanovic, S. Raicevic, Synthesis of antimicrobial monophase silverdoped hydroxyapatite nanopowders for bone tissue engineering, Appl. Surf. Sci. 257 (2011) 4510–4518. https://doi.org/10.1016/j.apsusc.2010.12.113.

[34] J. Kolmas, E. Groszyk, D. Kwiatkowska-Różycka, Substituted hydroxyapatites with antibacterial properties. Biomed Res. Int. (2014) 178123. https://doi.org/10.1155/2014/178123.

[35] B. Gayathri, N. Muthukumarasamy, D. Velauthapillai, S.B. Santhosh, V. Asokan, Magnesium incorporated hydroxyapatite nanoparticles: Preparation, characterization, antibacterial and larvicidal activity, Arab. J. Chem. 11 (2018), 645–654. https://doi.org/10.1016/j.arabjc.2016.05.010.

[36] V. Stanic, S. Dimitrijevic, J. Antic-Stankovic, M. Mitric, B. Jokic, I. B. Plecas, S. Raicevic, Synthesis, characterization and antimicrobial activity of copper and zinc-doped hydroxyapatite nanopowders. Appl. Surf. Sci. 256 (2010) 6083–6089. https://doi.org/10.1016/j.apsusc.2010.03.124.

[37] J. A. Lemire, J. J. Harrison, R. J. Turner, Antimicrobial activity of metals: mechanisms, molecular targets and applications, Nat. Rev. Microbiol. 11 (2013) 371–384. https://doi.org/10.1038/nrmicro3028.

[38] S. Shanmugam, B. Gopal, Copper substituted hydroxyapatite and fluorapatite: synthesis, characterization and antimicrobial properties, Ceram. Int. 40 (2014) 15655–15662. https://doi.org/10.1016/j.ceramint.2014.07.086.

[39] S.L. Warnes, C.W. Keevil, Mechanism of copper surface toxicity in vancomycin-resistant enterococci following wet or dry surface contact, Appl. Environ. Microbiol. 77 (2001) 6049–6059. https://doi.org/10.1128/AEM.00597-11.

[40] O. Soutourina, S. Dubrac, O. Poupel, T. Msadek, I. Martin-Verstraete, The pleiotropic CymR regulator of Staphylococcus aureus plays an important role in virulence and stress response, PLoS Pathog. 6 (2010), e1000894. https://doi.org/10.1371/journal.ppat.1000894.

[41] Z.X. Tang, B.F. Lv, MgO nanoparticles as antibacterial agent: preparation and activity, Braz. J. Chem. Eng. 31 (2014) 591–601. https://doi.org/10.1590/0104-6632.20140313s00002813.

[42] J. Sawai, Quantitative evaluation of antibacterial activities of metallic oxide powders (ZnO, MgO and CaO) by conductimetric assay, J. Microbiol. Methods 54 (2003) 177–182. https://doi.org/10.1016/S0167-7012(03)00037-X.

[43] N. Brändle, M. Zehnder, R. Weiger, T. Waltimo, Impact of growth conditions on susceptibility of five microbial species to alkaline stress, J. Endod. 34 (2008) 579–582. https://doi.org/10.1016/j.joen.2008.02.027.

[44] S. Gomes, C. Vichery, S. Descamps, H. Martinez, A. Kaur, A. Jacobs, J.M. Nedelec, G. Renaudin, Cu doping of calcium phosphate bioceramics: From mechanism to the control of cytotoxicity. Acta Biomater. 65 (2018) 462–474. https://doi.org/10.1016/j.actbio.2017.10.028.

[45] G.D. Webler, A.C.C.Correia, E. Barreto, E.J.S.Fonseca, Mg-doped biphasic calcium phosphate by a solid state reaction route: Characterization and evaluation of

cytotoxicity, Mater. Chem. Phys. 162 (2015) 177–181. https://doi.org/10.1016/j.matchemphys.2015.05.055.

[46] R.C. Richard, J. Dai, M.S. Sader, G.A. Soares, R.M.S.M. Thiré, Characterization of β-TCP, β-TCMP and BCMP Produced by Hydrolysis, Bioceram. Dev. Appl. (2013) S1: 001. doi: 10.4172/2090-5025.S1-001. https://doi.org/10.4172/2090-5025.S1-001.

[47] G. Liangzhi, Z. Weibin S. Yuhui, Magnesium substituted hydroxyapatite whiskers: synthesis, characterization and bioactivity evaluation, RSC Adv. 6 (2016) 114707. https://doi.org/ 10.1039/C6RA24469F.

[48] J.C. Elliott, Structure and chemistry of the apatites and other calcium orthophosphates, Elsevier, Amsterdam, 1994.

[49] M. Frasnelli, V.M. Sglavo, Effect of Mg doping on beta-alpha phase transition in TCP bioceramics, Acta Biomater. 33 (2016) 283–289. https://doi.org/10.1016/j.actbio.2016.01.015.

[50] S.V. Dorozhkin, Biphasic, triphasic and multiphasic calcium orthophosphates, Acta Biomater. 8 (2012) 963–977. https://doi.org/10.1016/j.actbio.2011.09.003.

[51] R. Enderle, F. Götz-Neunhoeffer, M. Göbbels, F.A. Müller, P. Greil, Influece of magnesium doping on the phase transformation temperature of β–TCP ceramics examined by Rietveld refinement, Biomaterials 26 (2005) 3379–3384. https://doi.org/10.1016/j.biomaterials.2004.09.017.

[52] L. Stipniece,V. Stepanova, I. Narkevica, K. Salma-Ancane, A.R. Boyd, Comparative study of surface properties of Mg-substituted hydroxyapatite bioceramic microspheres, J. Eur. Cer. Soc. 38 (2018) 761–768. https://doi.org/10.1016/j.jeurceramsoc.2017.09.026.

[53] S.J. Kalita, H.A. Bhatt, Nanocrystalline hydroxyapatite doped with magnesium and zinc: synthesis and characterization, Mater. Sci. Eng. C 27 (2007) 837–848. https://doi.org/10.1016/j.msec.2006.09.036.

[54] Z. Radovanovic, Dj. Veljovic, L. Radovanovic, I. Zalite, E. Palcevskis, R. Petrovic, Dj. Janackovic, Ag^{+}, Cu^{2+} and Zn^{2+} doped hydroxyapatite/tricalcium phosphate bioceramics: Influence of doping and sintering technique on mechanical properties, Process. Appl. Ceram. 12 (2018) 268–276. https://doi.org/ 10.2298/PAC1803268R.

[55] Dj. Veljovic, E. Palcevskis, A. Dindune, S. Putic, I Balac, R. Petrovic, Dj Janackovic, Microwave sintering improves the mechanical properties of biphasic calcium phosphates from hydroxyapatite microspheres produced from hydrothermal processing, J. Mater. Sci 45 (2010) 3175–3183. https://doi.org/10.1007/s10853-010-4324-8.

[56] D.J. Curran, T.J. Fleming, M.R. Towler, S. Hampshire, Mechanical parameters of strontium doped hydroxyapatite sintered using microwave and conventional methods, J. Mechan. Behav. Biomed. Mater. 4 (2011) 2063–2073. https://doi.org/10.1016/j.jmbbm.2011.07.005.

[57] M. Lukic, Z.S. Stojanovic, S.D. Skapin, M. Macek-Krzmanc, M. Mitric, S Markovic, D. Uskokovic, Dense fine-grained biphasic calcium phosphate (BCP) bioceramics designed by two-step sintering. J. Eur. Ceram. Soc. 31 (2011) 19–27. https://doi.org/10.1016/j.jeurceramsoc.2010.09.006.

[58] J. Wang, L. L Shaw, Nanocrystalline hydroxyapatite with simultaneous enhancements in hardness and toughness, Biomaterials 30 (2009) 6565–6572. https://doi.org/10.1016/j.biomaterials.2009.08.048.

[59] Dj. Veljovic, B. Jokic, R. Petrovic, E. Palcevskis, A. Dindune, I.N. Mihailescu, Dj. Janackovic, Processing of dense nanostructured HAP ceramics by sintering and hot pressing, Ceram. Int. 35 (2009) 1407–1413. https://doi.org/10.1016/j.ceramint.2008.07.007.

[60] S. Li, H. Izui, M. Okano, Densification, microstructure and behavior of hydroxyapatite ceramics sintered by using spark plasma sintering, J. Eng. Mater. Technol. 130 (2008) 031012-1–031012-7. https://doi.org/10.1115/1.2931153.

[61] Dj.Veljovic, R. Jancic-Hajneman, I. Balac, B. Jokic, S. Putic, R. Petrovic, Dj. Janackovic, The effect of the shape and size of the pores on the mechanical properties of porous HAP-based bioceramics, Ceram. Int. 37 (2011) 471–479. https://doi.org/10.1016/j.ceramint.2010.09.014.

Fig. 1. *XRD patterns of the as-prepared powder samples*

Fig. 2. *SEM micrographs of the obtained powders: a)HAP1; b)HAP5; c)HAP7.5; d)HAP10; e)HAP15; f)HAP20*

Fig. 3. *Results of the MTT assay performed on: a) MRC-5; b) L929 cell line*

Fig. 4. *a) TGA and b) DTA curves of the samples*

Fig. 5. *Dilatometric curves*

Fig. 6. *XRD patterns of the sintered samples: c-HAP-HAP7.5 (1200 °C); HAP10 (1000 °C); HAP15, HAP20 (750 °C)*

Fig. 7. *Microstructure of the Mg,Cu-HAP sintered samples: a)HAP0 (1200 °C); b)HAP1 (1200 °C); c)HAP5 (1200 °C); d)HAP7.5 (1200 °C); e)HAP10 (1000 °C); f)HAP15 (750 °C); g)HAP20 (750 °C)*

Fig. 8. *SEM micrographs of etched samples sintered at 1200 °C: a) HAP0; b) HAP1; c) HAP5*

Fig. 9. *Hardness by Vickers of the sintered Mg,Cu-HAP samples*

Fig. 10. *Fracture toughness of the sintered Mg,Cu-HAP samples*

Table 2. *The composition of precursor solutions for hydrothermal synthesis of each sample*

Sample (composition)	$Ca(NO_3)_2 \cdot 4H_2O$ (g)	$Na_2H_2EDTA \cdot 2H_2O$ (g)	$NaH_2PO_4 \cdot 2H_2O$ (g)	Urea (g)	$Mg(NO_3)_2 \cdot 6H_2O$ (g)	$Cu(NO_3)_2 \cdot 3H_2O$ (g)
c-HAP (0 mol.% Cu, 0 mol.% Mg)	11.80 (0.05 mol)	11.18	4.68 (0.03 mol)	12.00	0 (0.00 mol)	0 (0.00 mol)
HAP0 (0.4 mol.% Cu, 0 mol.% Mg)	11.76 (0.0498 mol)	11.18	4.68 (0.03 mol)	12.00	0 (0.00 mol)	0.0483 (0.0002 mol)
HAP1 (0.4 mol.% Cu, 1 mol.% Mg)	11.64 (0.0493 mol)	11.18	4.68 (0.03 mol)	12.00	0.128 (0.0005 mol)	0.0483 (0.0002 mol)
HAP5 (0.4 mol.% Cu, 5 mol.% Mg)	11.17 (0.0473 mol)	11.18	4.68 (0.03 mol)	12.00	0.641 (0.0025 mol)	0.0483 (0.0002 mol)
HAP7.5 (0.4 mol.% Cu, 7.5 mol.% Mg)	10.87 (0.04605 mol)	11.18	4.68 (0.03 mol)	12.00	0.962 (0.00375 mol)	0.0483 (0.0002 mol)
HAP10 (0.4 mol.% Cu, 10 mol.% Mg)	10.58 (0.0448 mol)	11.18	4.68 (0.03 mol)	12.00	1.282 (0.005 mol)	0.0483 (0.0002 mol)
HAP15 (0.4 mol.% Cu, 15 mol.% Mg)	9.98 (0.0423 mol)	11.18	4.68 (0.03 mol)	12.00	1.923 (0.0075 mol)	0.0483 (0.0002 mol)
HAP20 (0.4 mol.% Cu, 20 mol.% Mg)	9.40 (0.0398 mol)	11.18	4.68 (0.03 mol)	12.00	2.564 (0.01 mol)	0.0483 (0.0002 mol)

Table 2. *Elemental composition of the obtained powders*

Ions / Sample	Ca [at. %]	P [at. %]	Mg [at. %]	Cu [at. %]	Ca / P ratio	(Ca+Mg+Cu)/P ratio
HAP1	13.13	8.58	0.04	0.04	1.53	1.54
HAP5	11.58	7.97	0.25	0.03	1.45	1.49
HAP7.5	13.06	9.67	0.68	0.03	1.35	1.42
HAP10	11.67	9.02	0.85	0.02	1.29	1.39
HAP15	10.55	8.70	1.20	0.03	1.22	1.35
HAP20	11.35	9.26	1.35	0.00	1.21	1.37

Table 3. *Results of antibacterial activity of the samples*

Sample	*E. coli*	*E. faecalis*	*S.aureus*
	degree of inhibition, *R* [%]		
c-HAP	/	/	/
HAP0	65.57	51.72	61.54
HAP1	65.29	57.93	66.74
HAP5	65.87	51.72	71.19
HAP10	57.31	34.48	76.03
HAP15	50.59	26.21	92.49
HAP20	50.18	21.38	97.67

Table 4. *Density and relative linear shrinkage of the sintered samples*

Sample	ρ [g/cm^3]	*RLS* [%]
c-HAP	2.54	15.00
HAP0	2.56	15.00
HAP1	2.82	16.88
HAP5	3.01	17.50
HAP10	2.07	9.38

Figure 1

Click here to download high resolution image

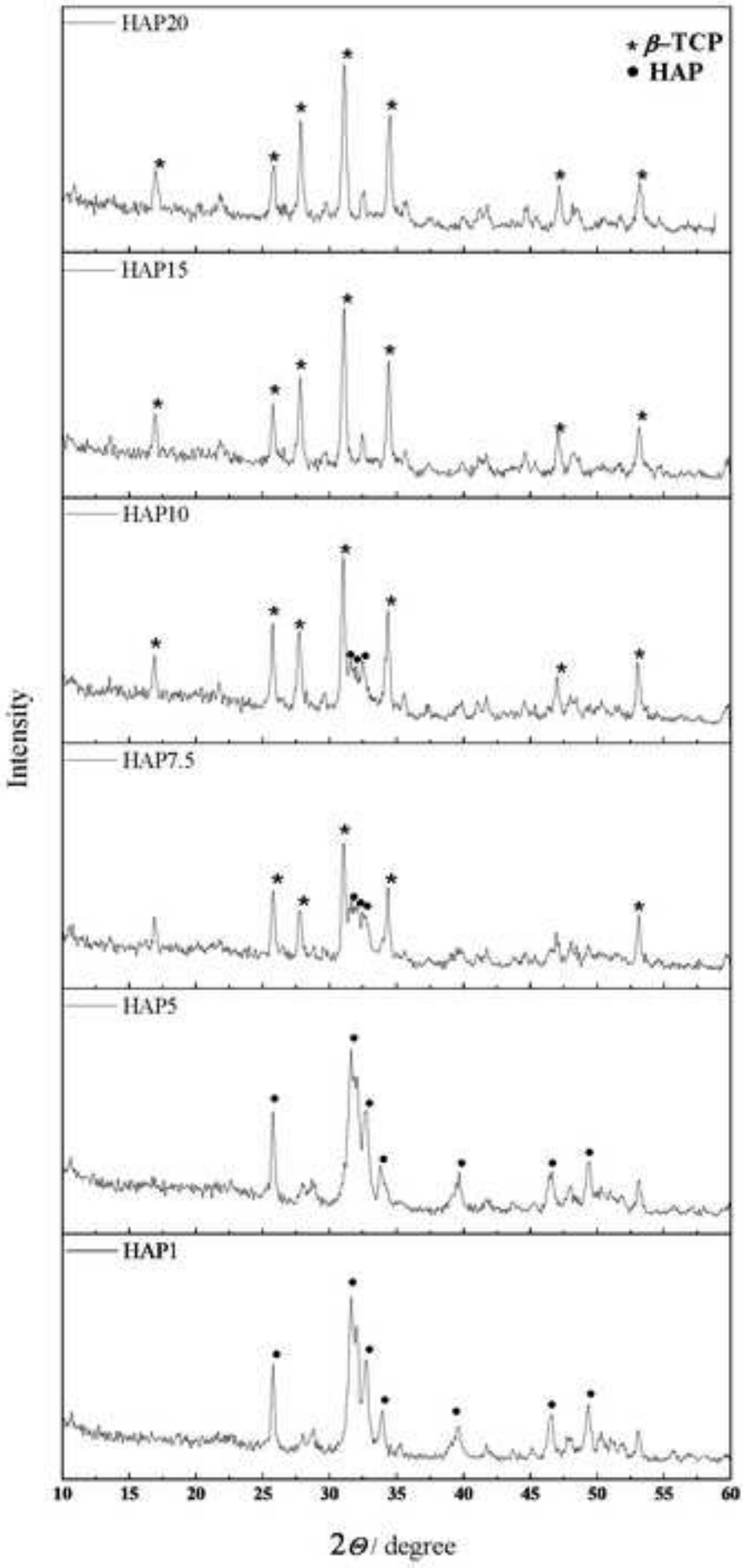

Figure 2a

Click here to download high resolution image

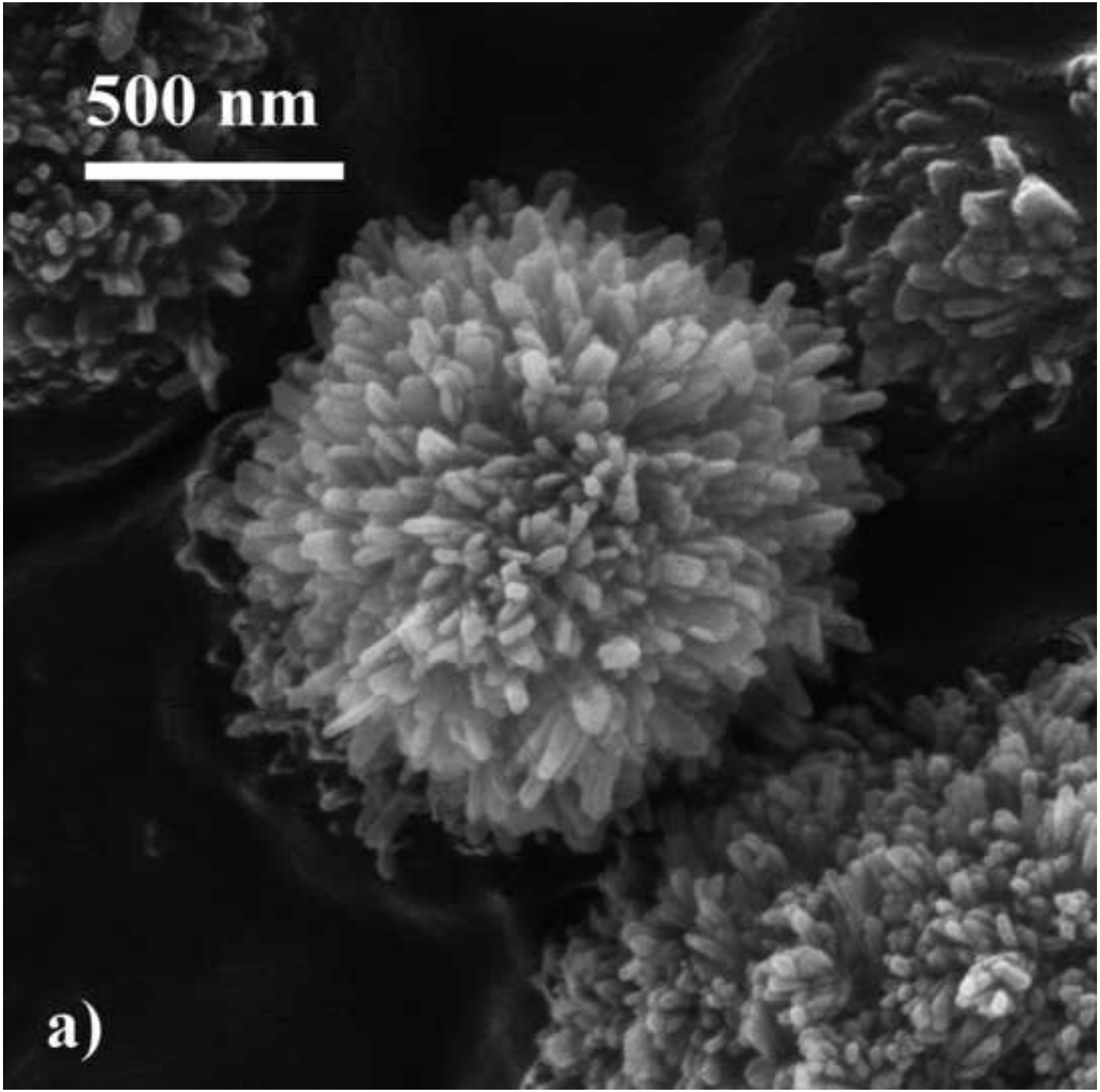

Figure 2b

Click here to download high resolution image

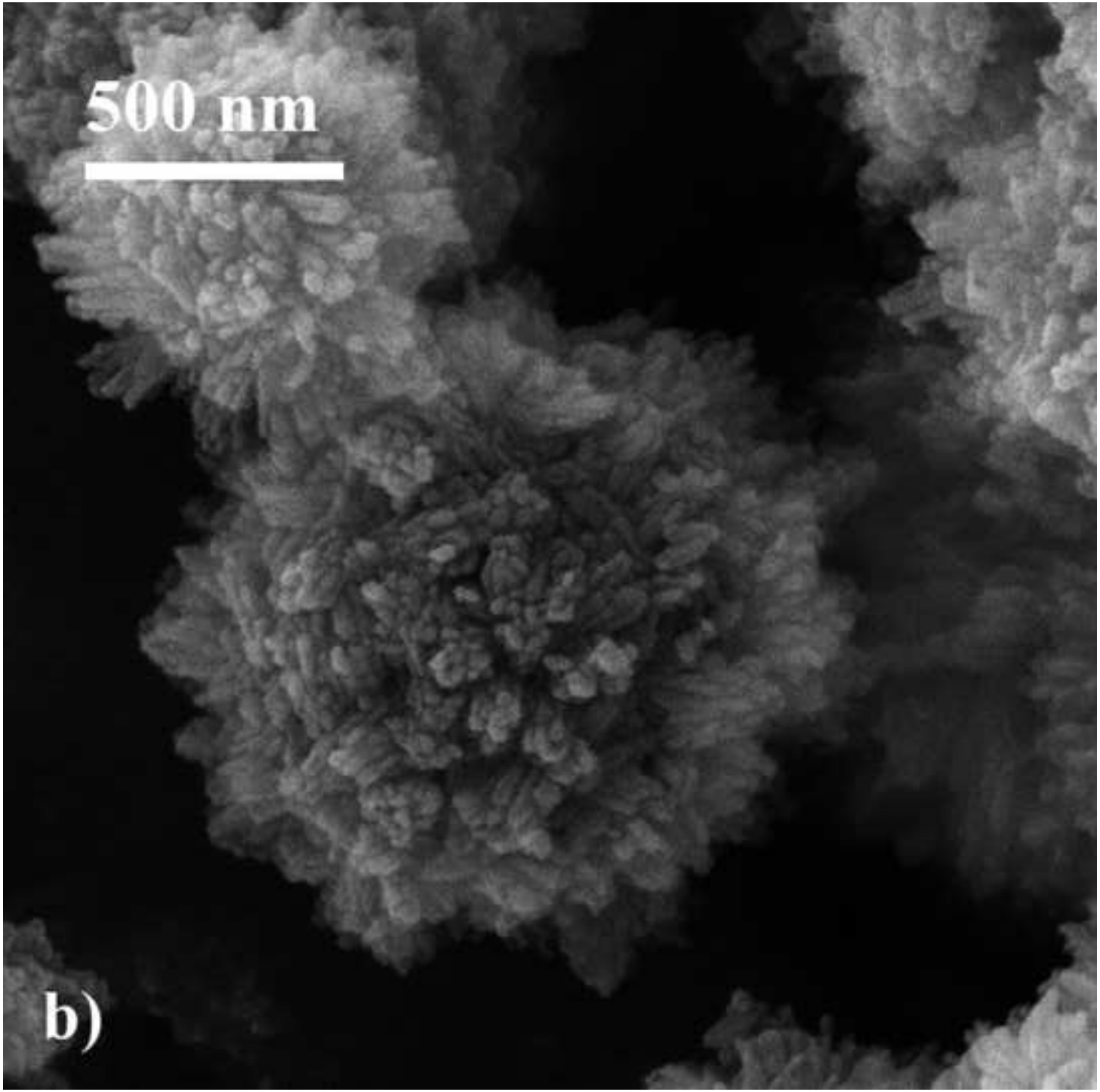

Figure 2c

Click here to download high resolution image

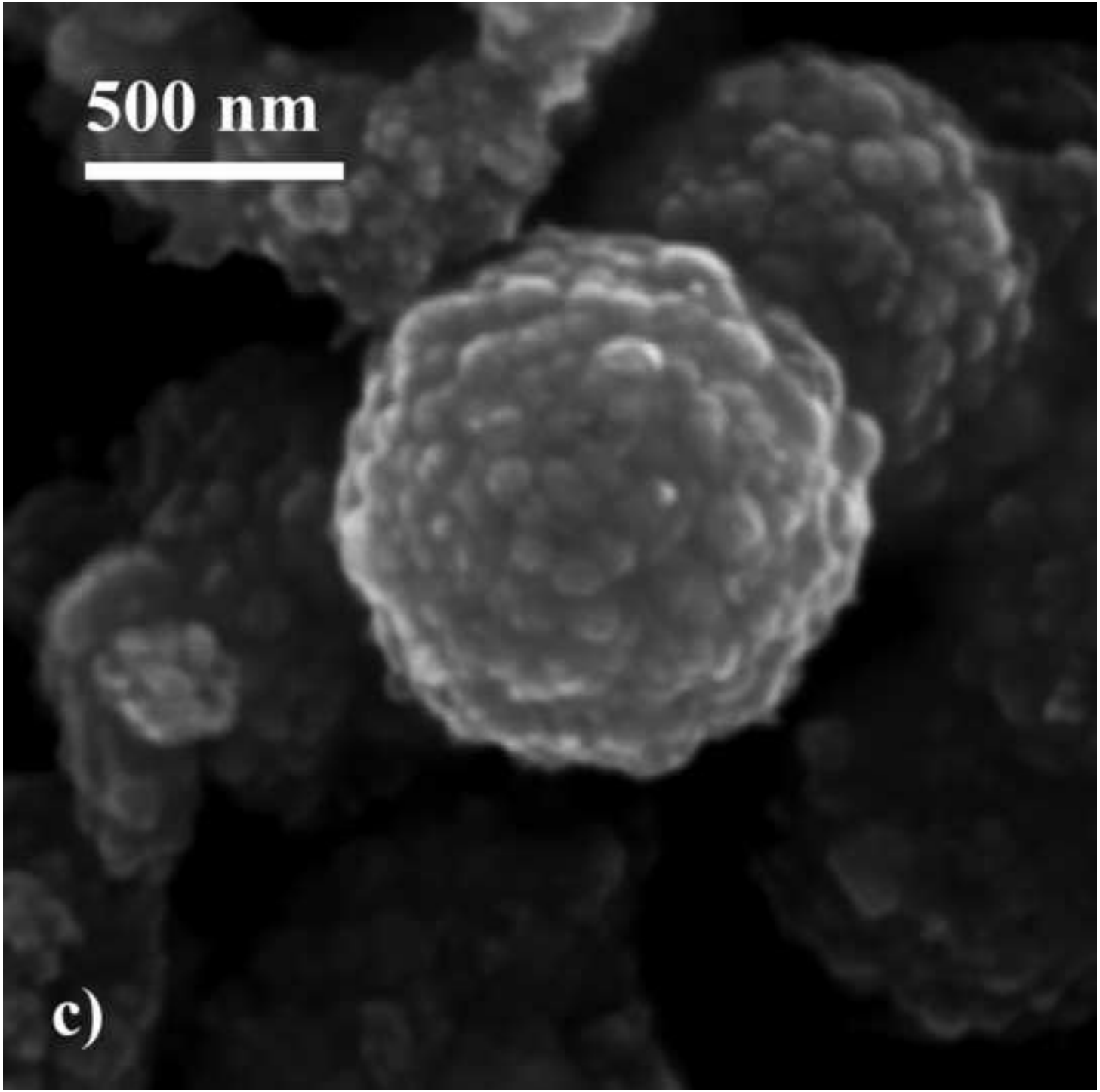

Figure 2d

Click here to download high resolution image

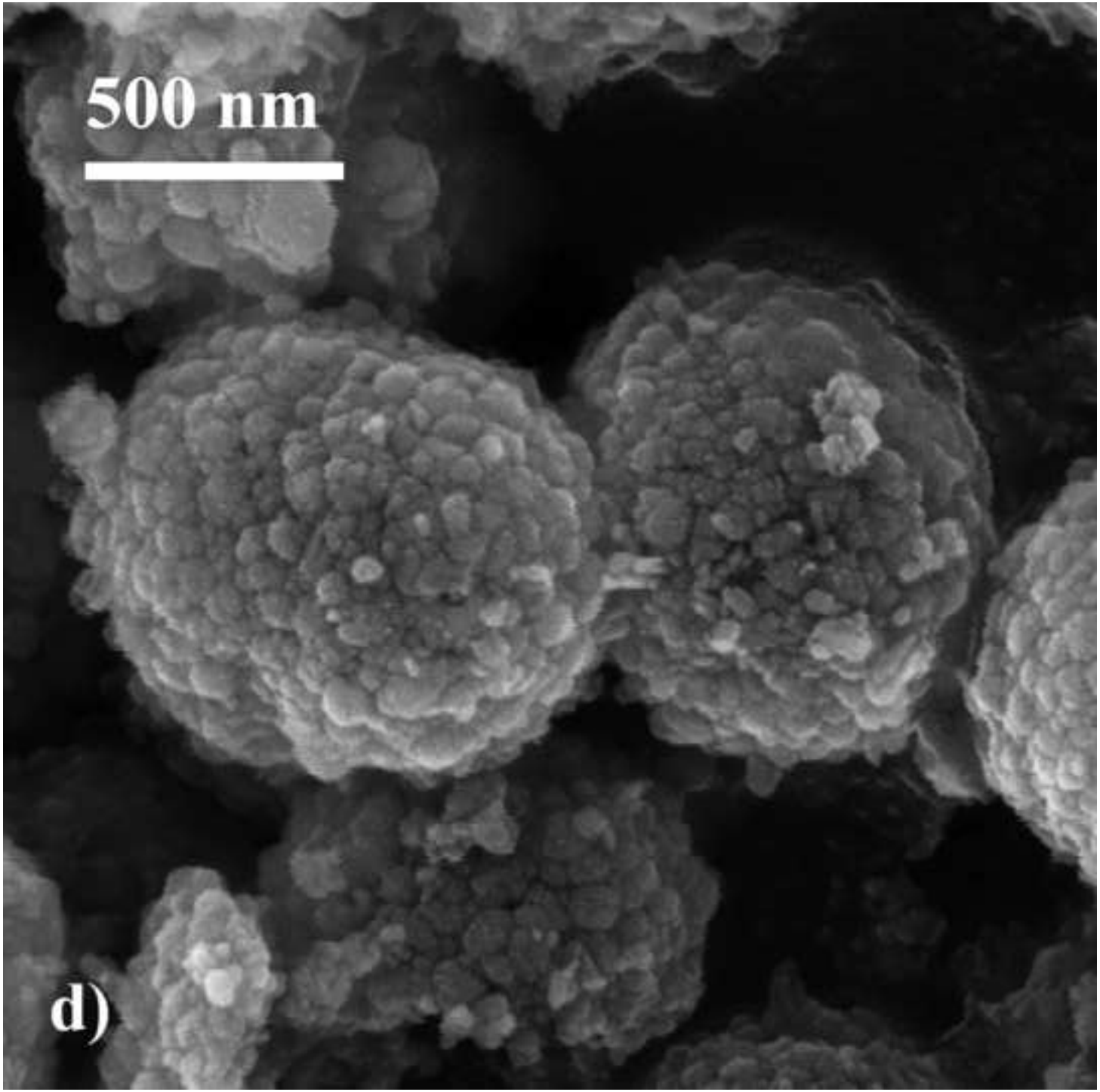

Figure 2e

Click here to download high resolution image

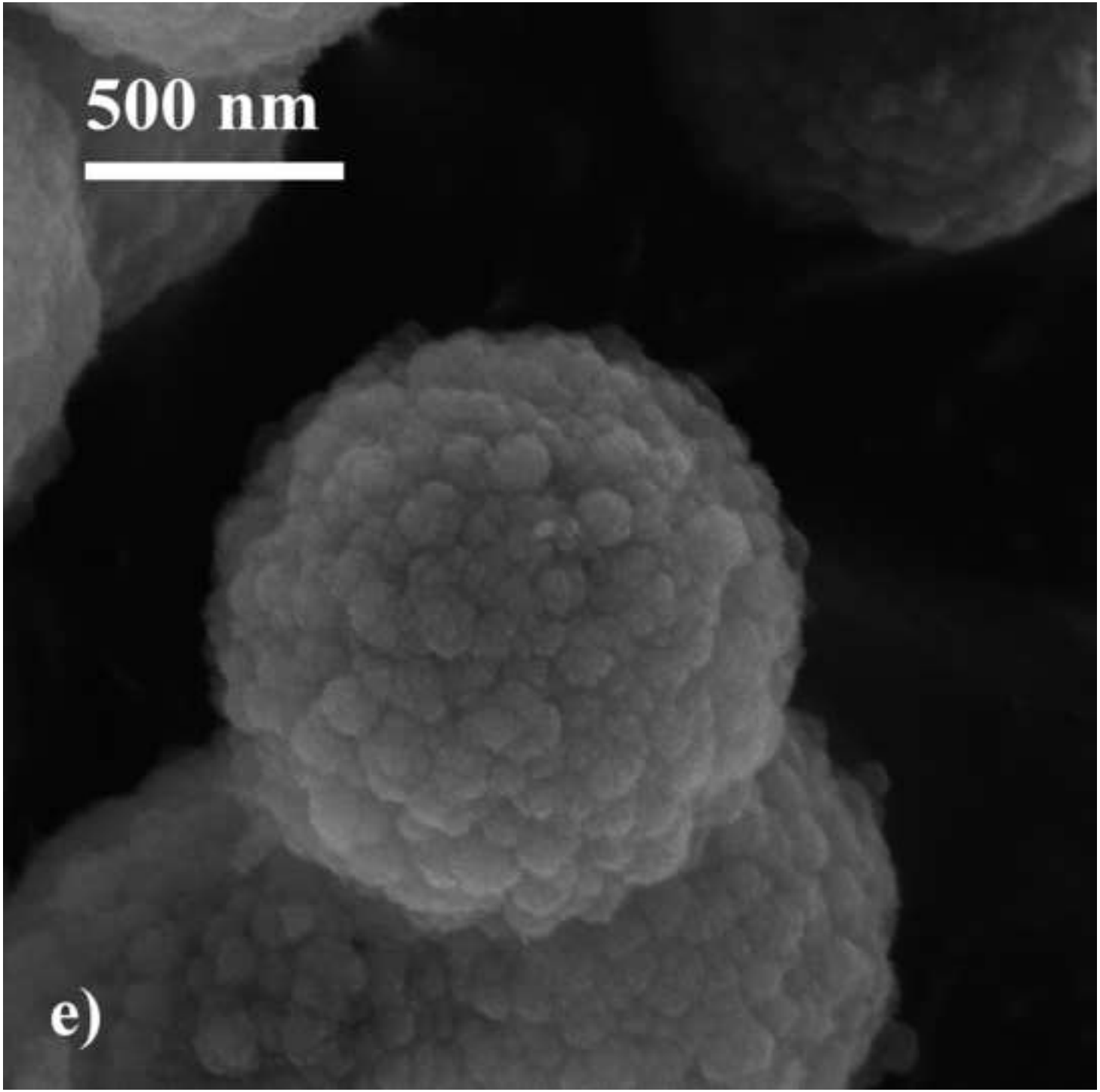

Figure 2f

Click here to download high resolution image

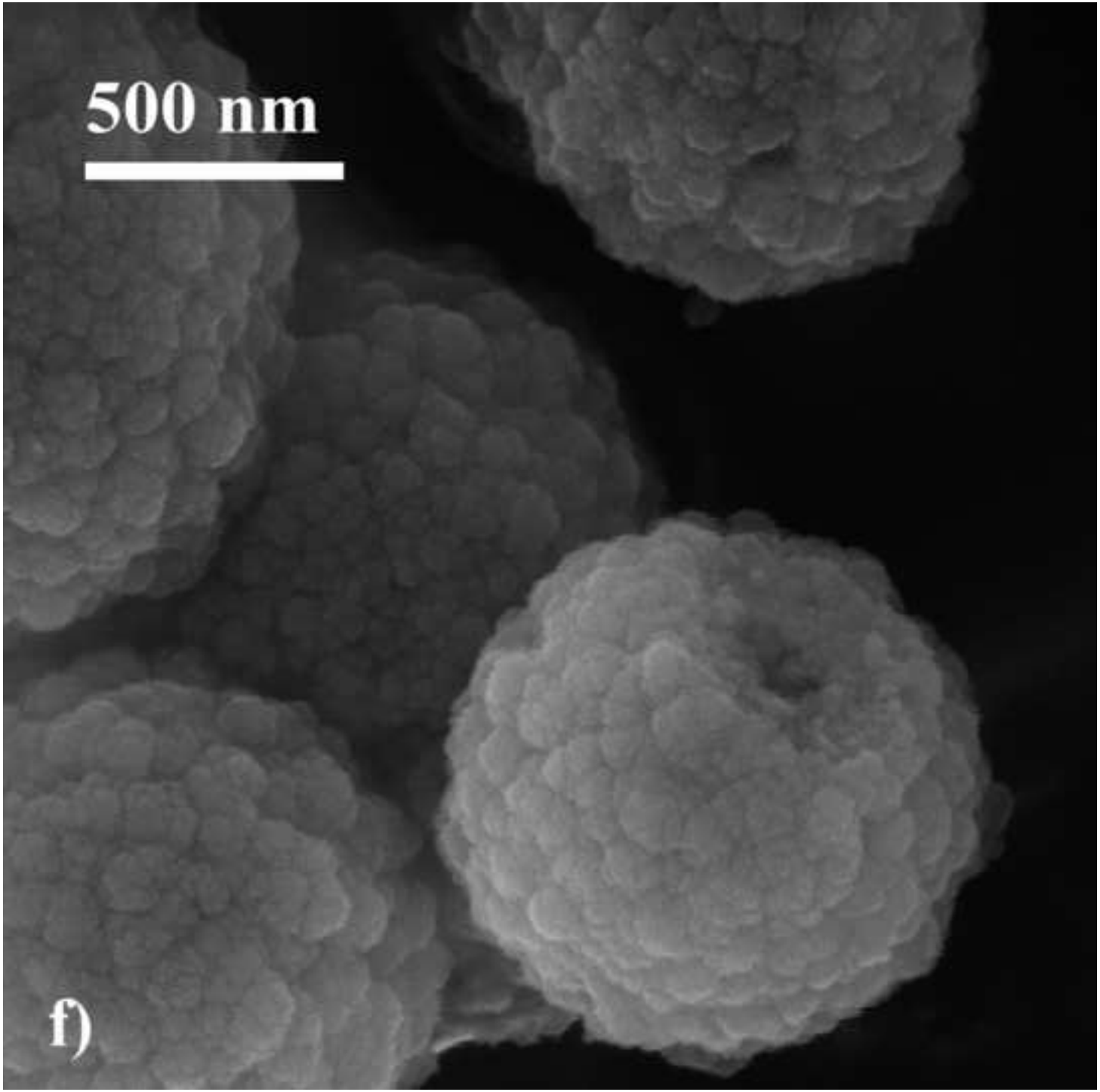

Figure 3a

Click here to download high resolution image

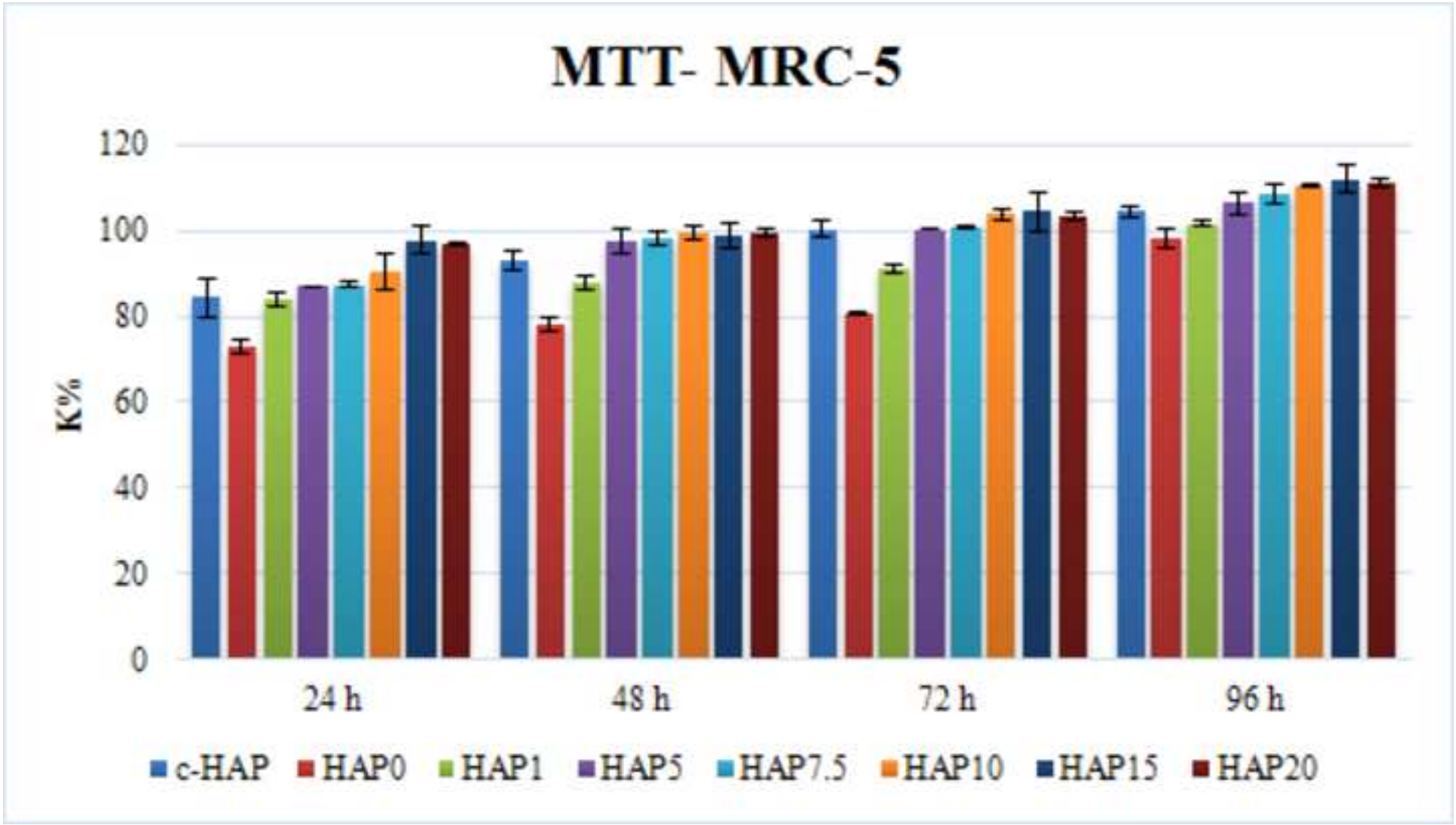

Figure 3b

Click here to download high resolution image

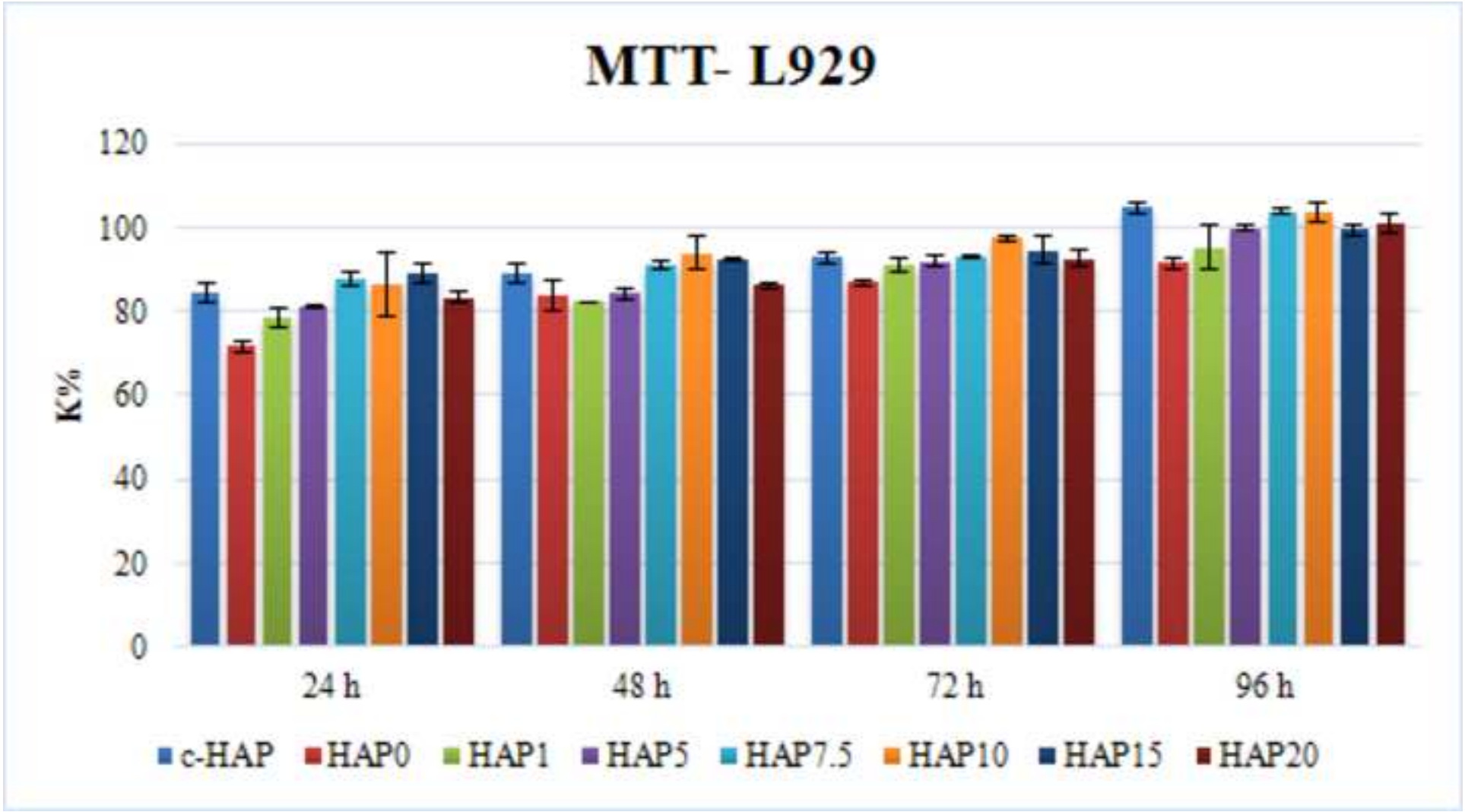

Figure 4a

Click here to download high resolution image

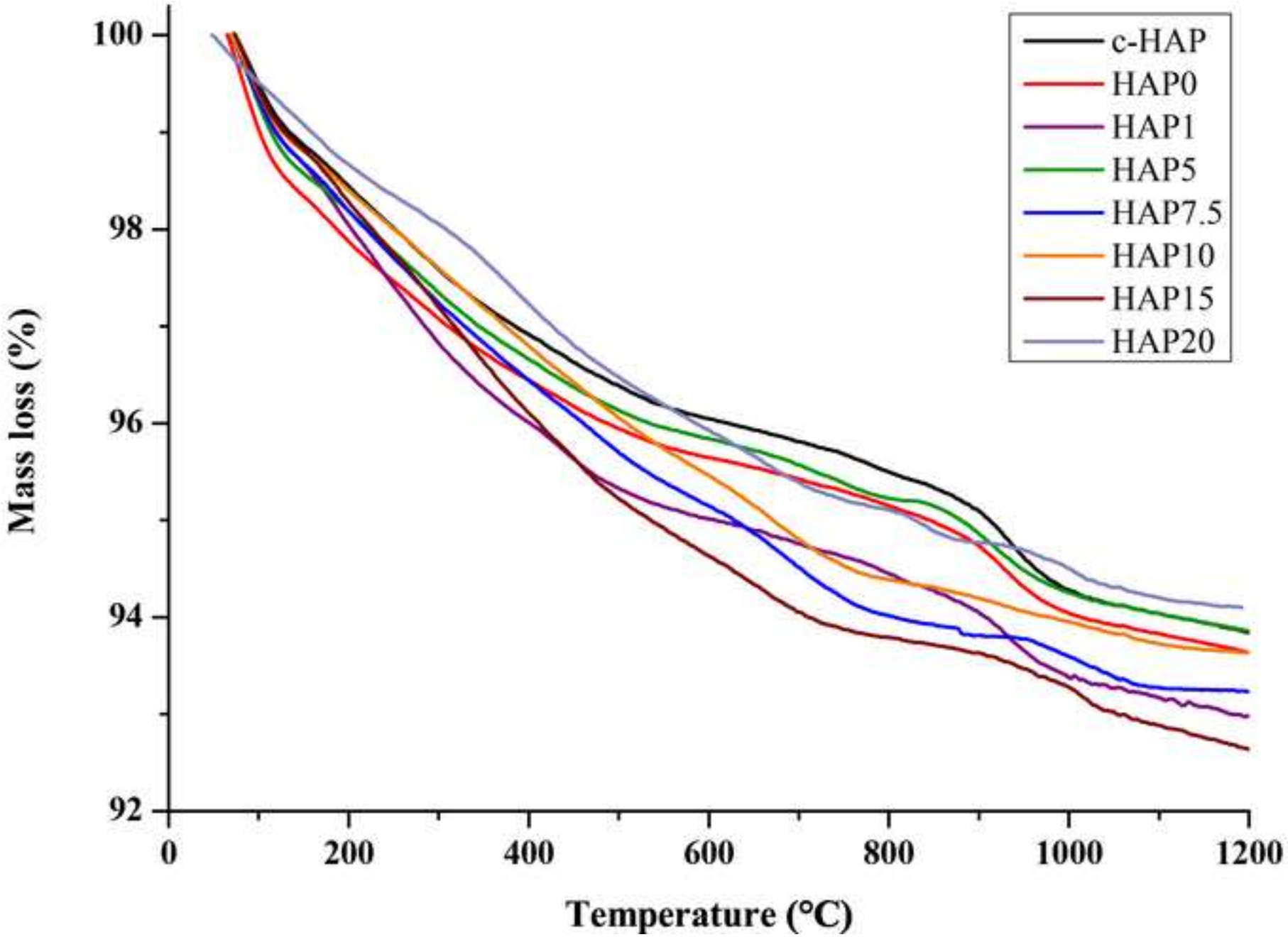

Figure 4b

Click here to download high resolution image

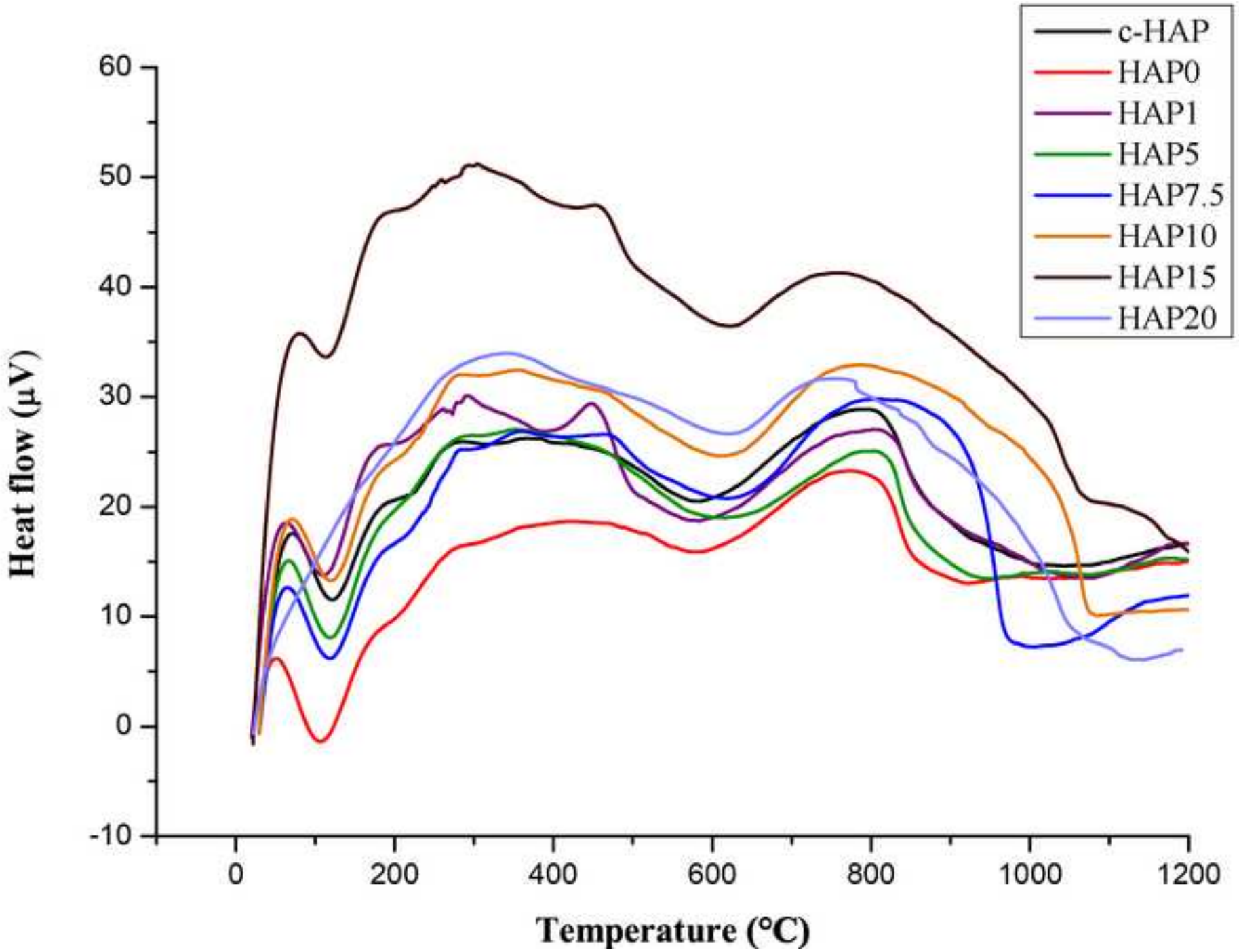

Figure 5

Click here to download high resolution image

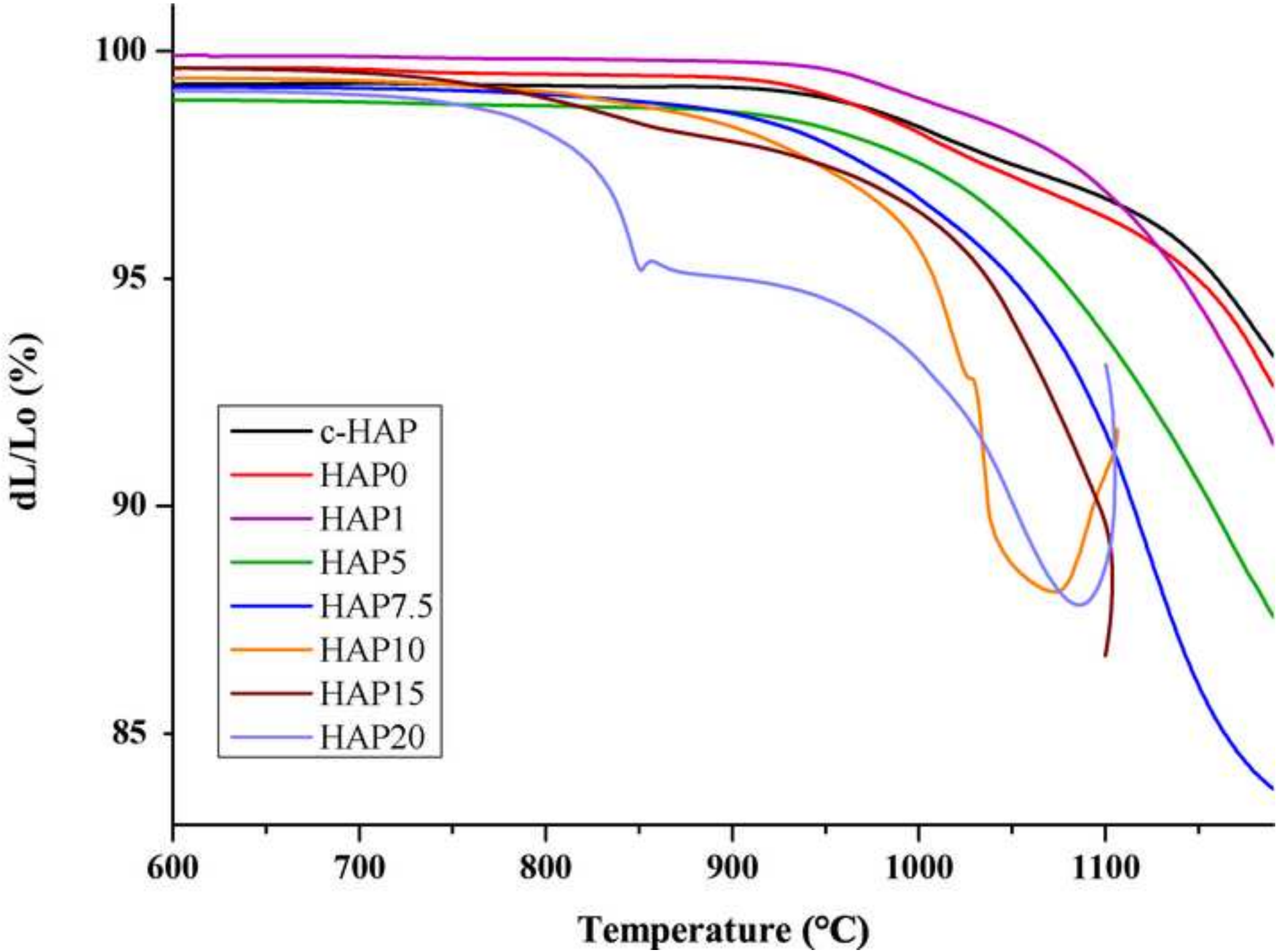

Figure 6

Click here to download high resolution image

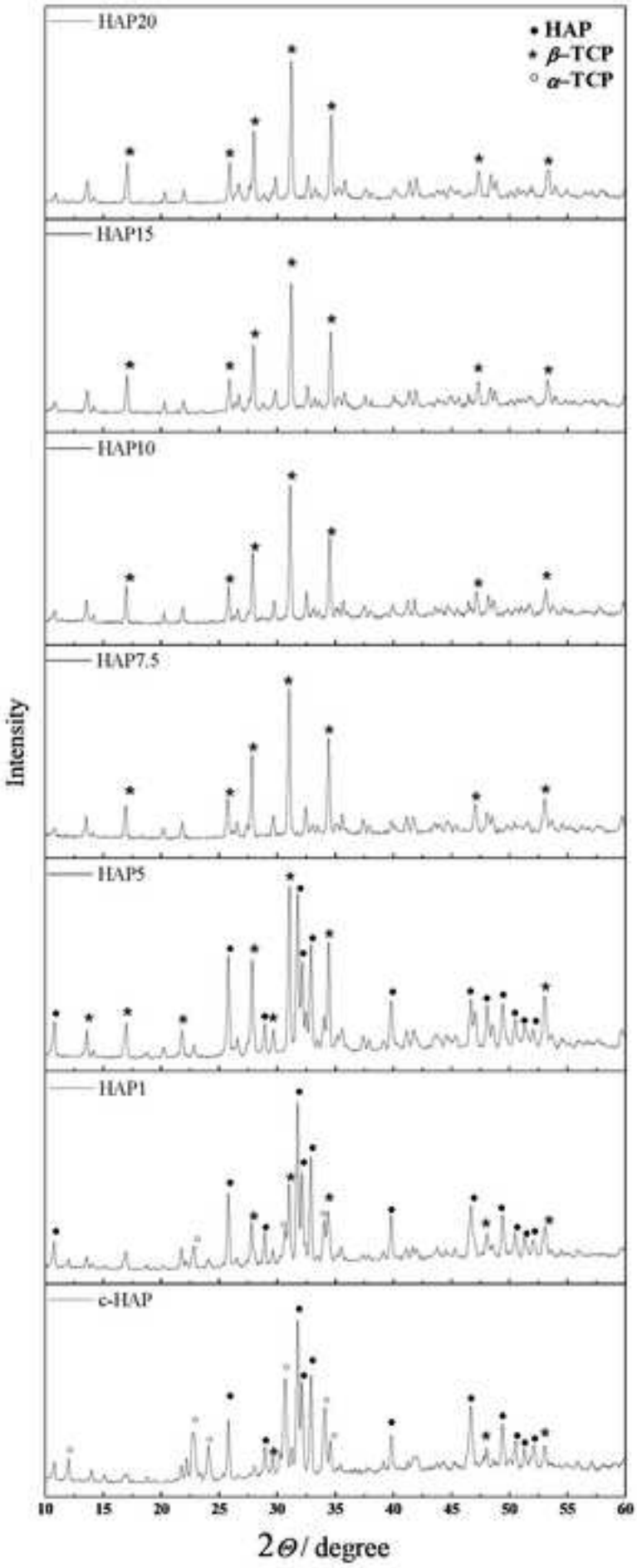

Figure 7a

Click here to download high resolution image

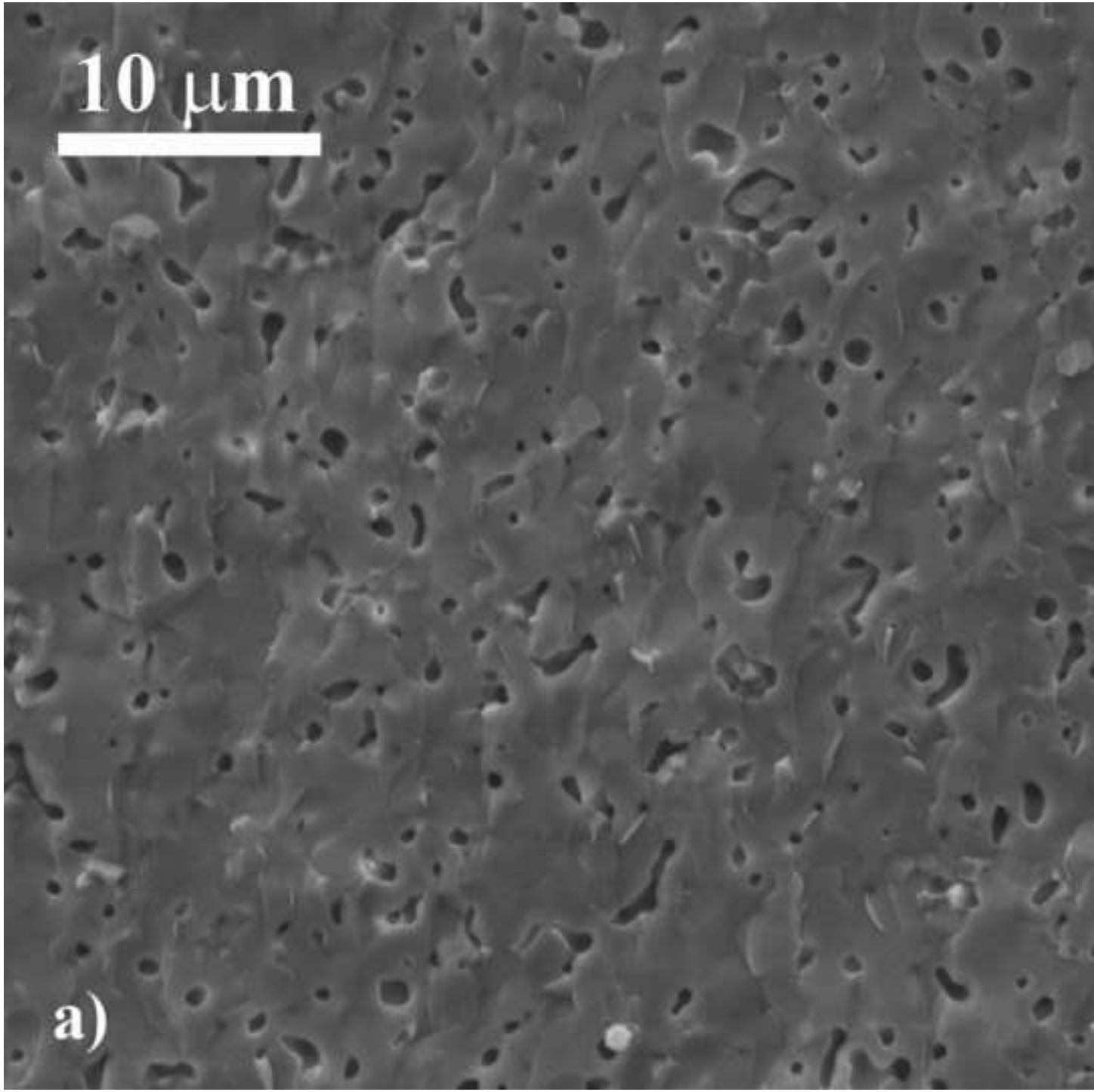

Figure 7b

Click here to download high resolution image

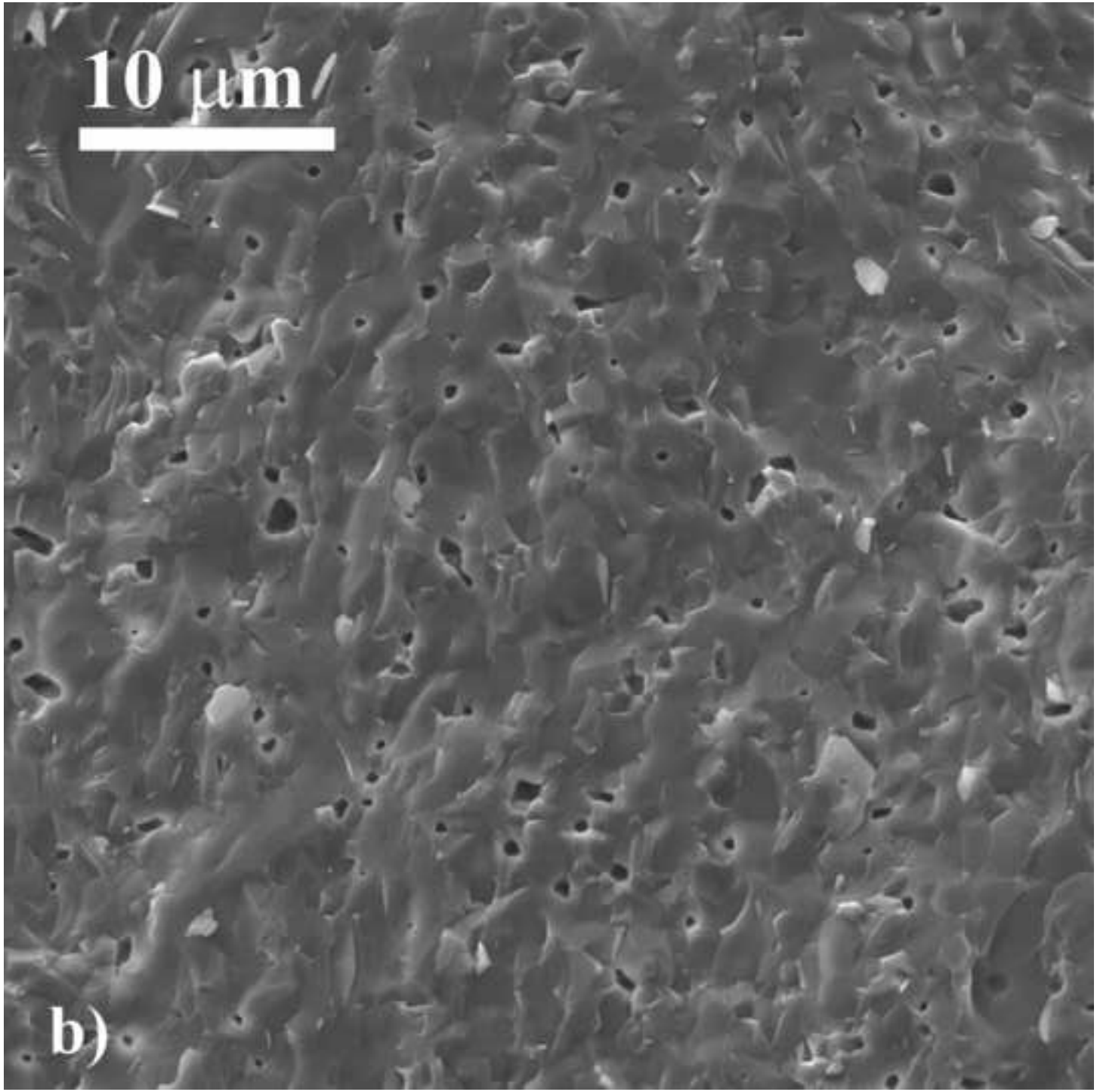

Figure 7c

Click here to download high resolution image

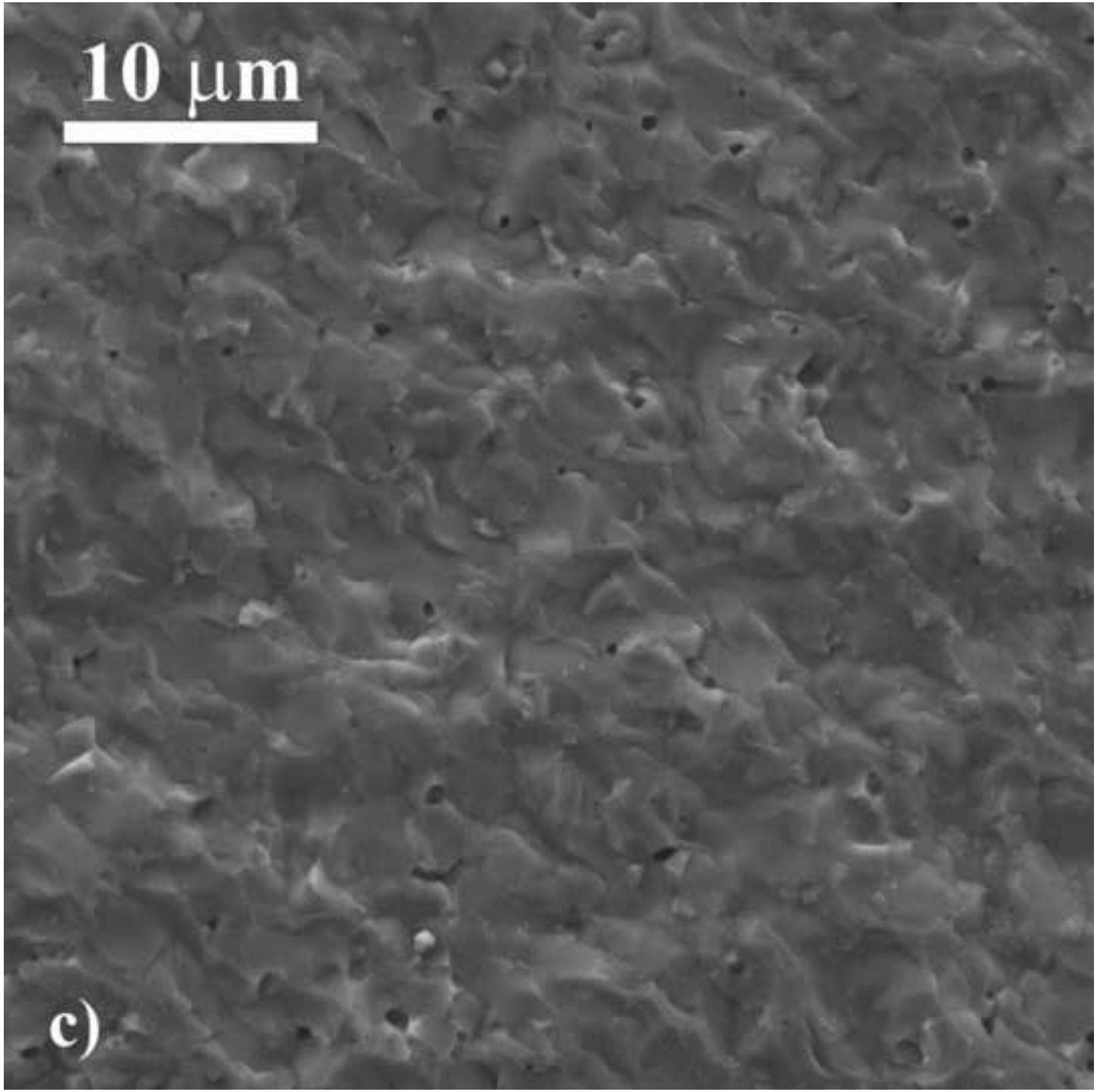

Figure 7d

Click here to download high resolution image

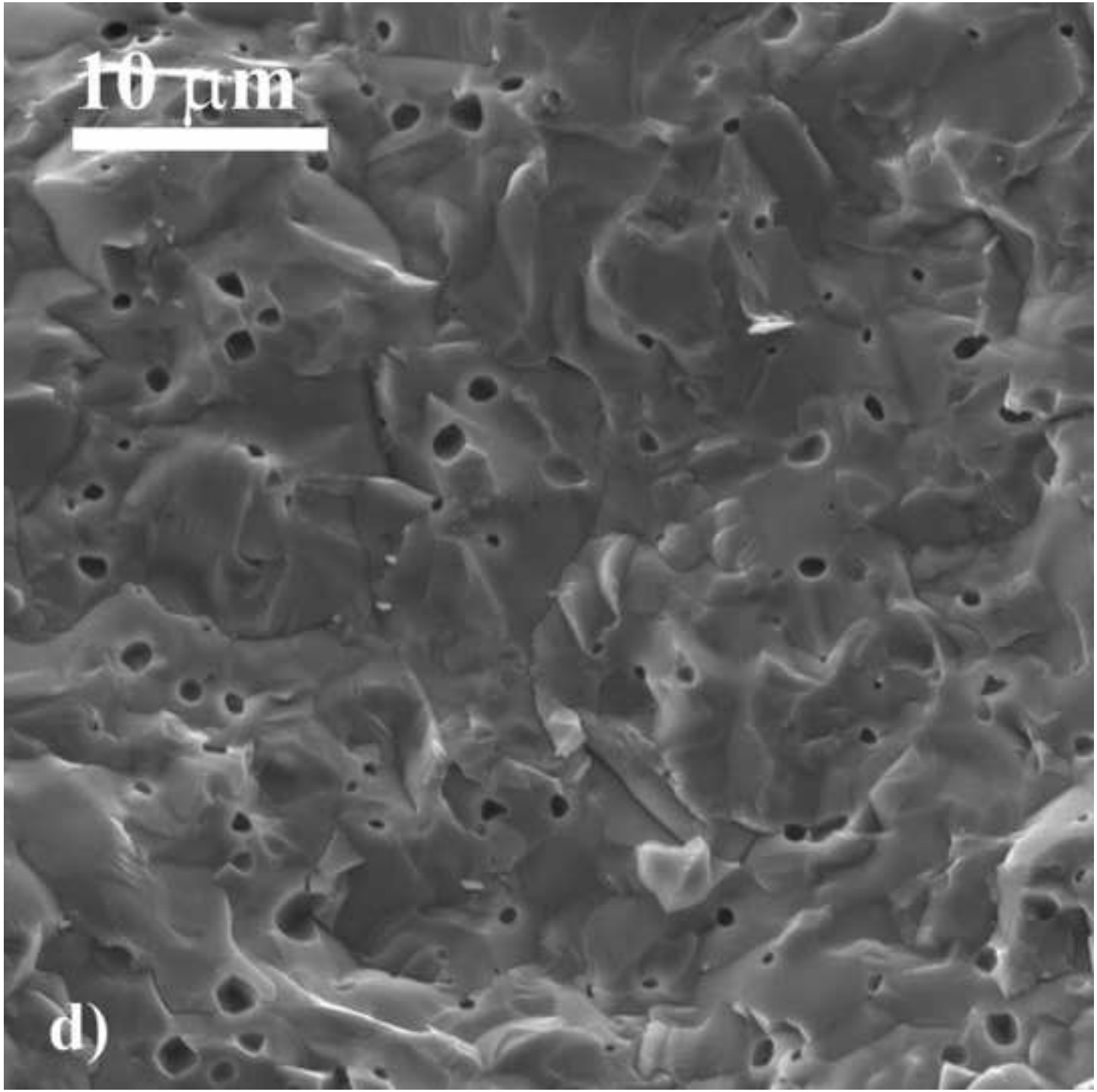

Figure 7e

Click here to download high resolution image

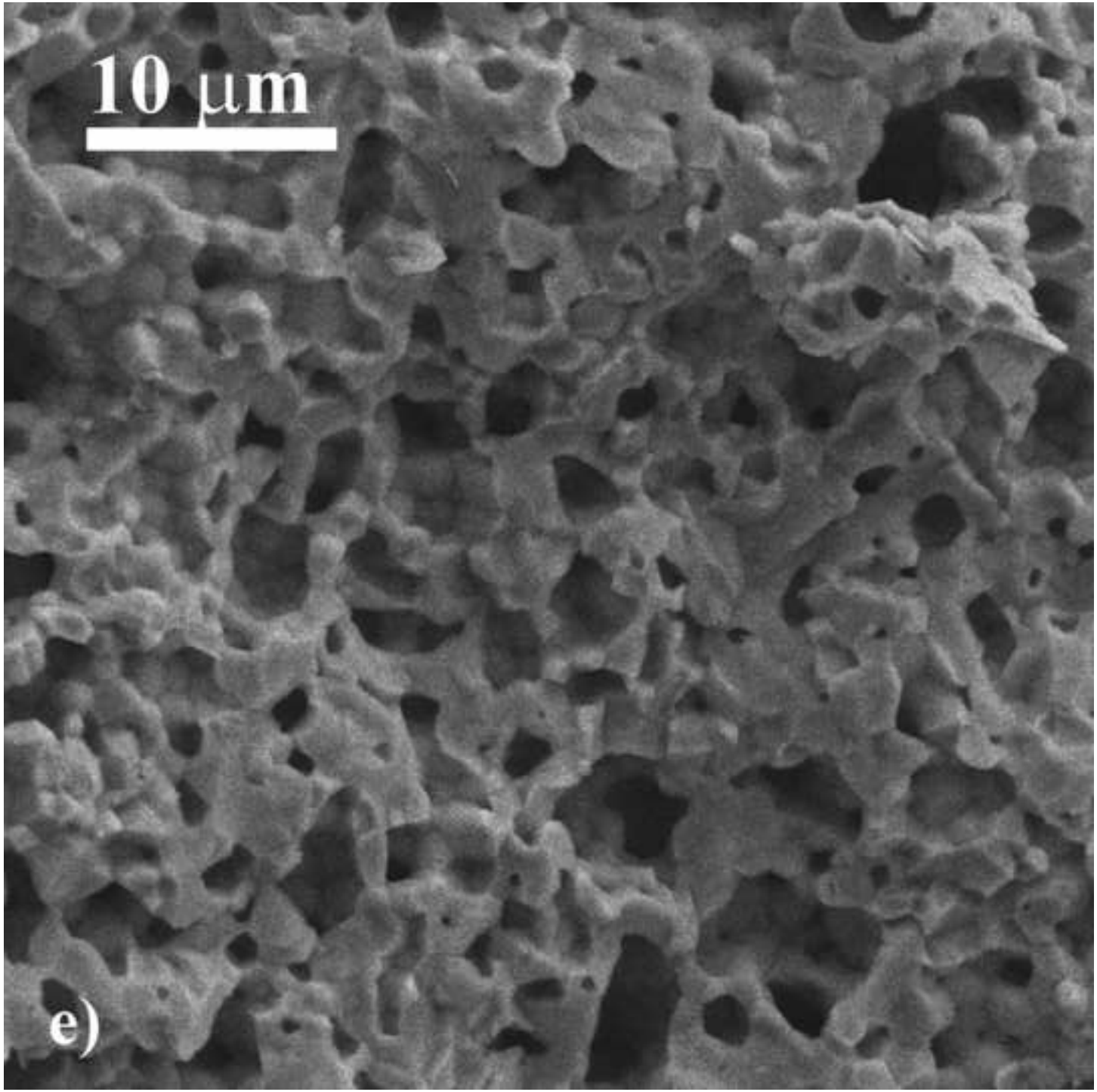

Figure 7f

Click here to download high resolution image

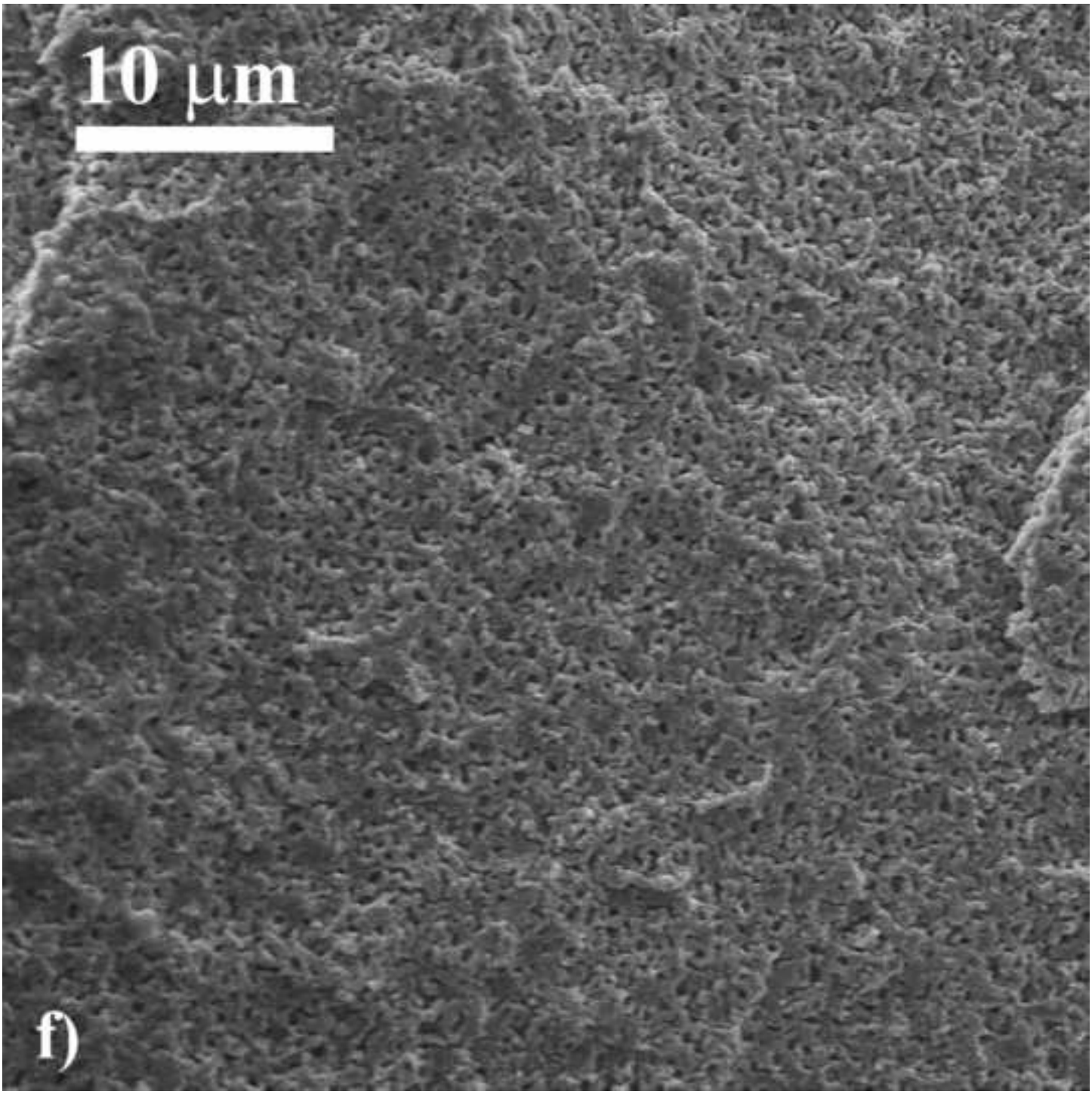

Figure 7g

Click here to download high resolution image

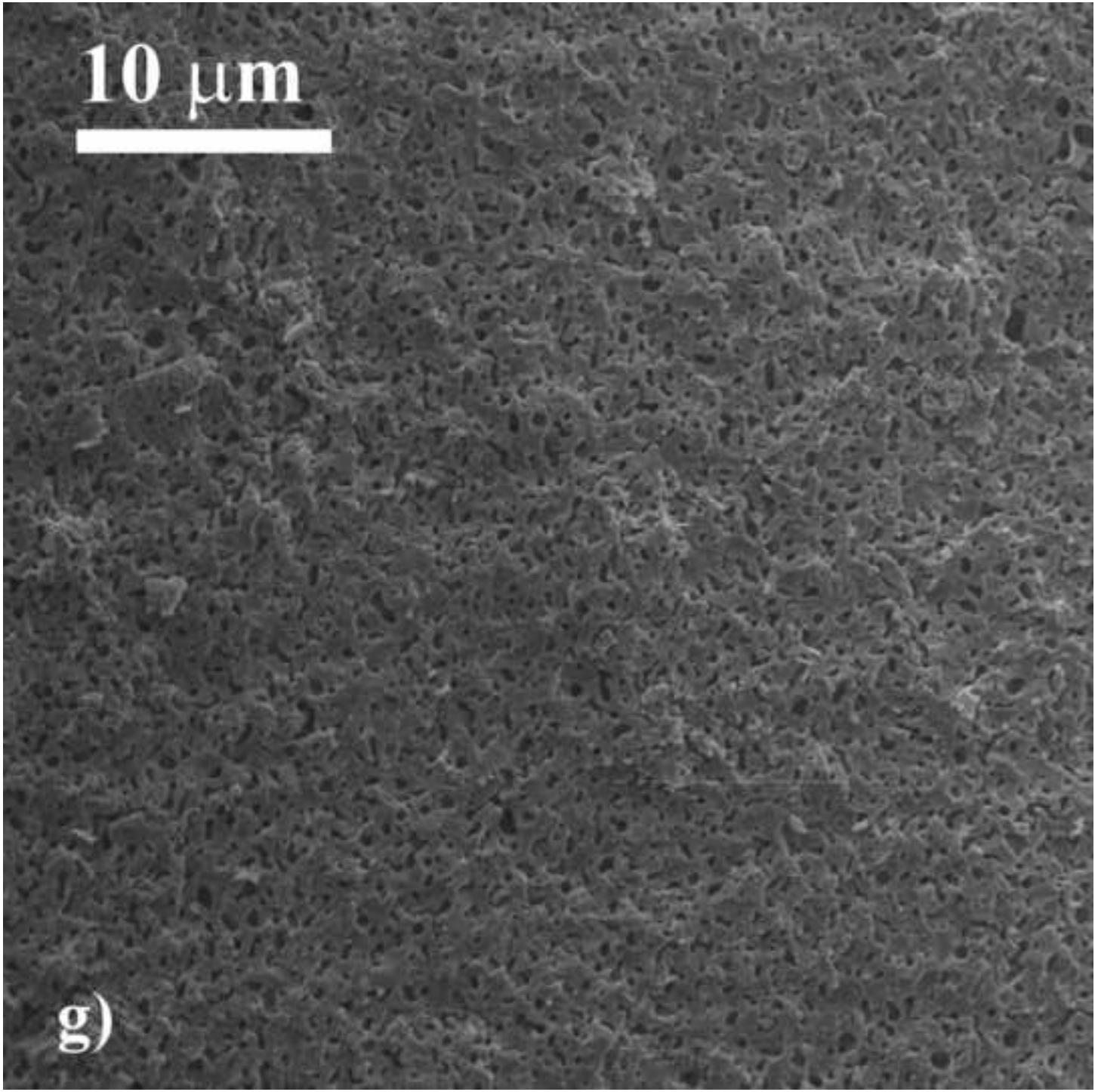

Figure 8a

Click here to download high resolution image

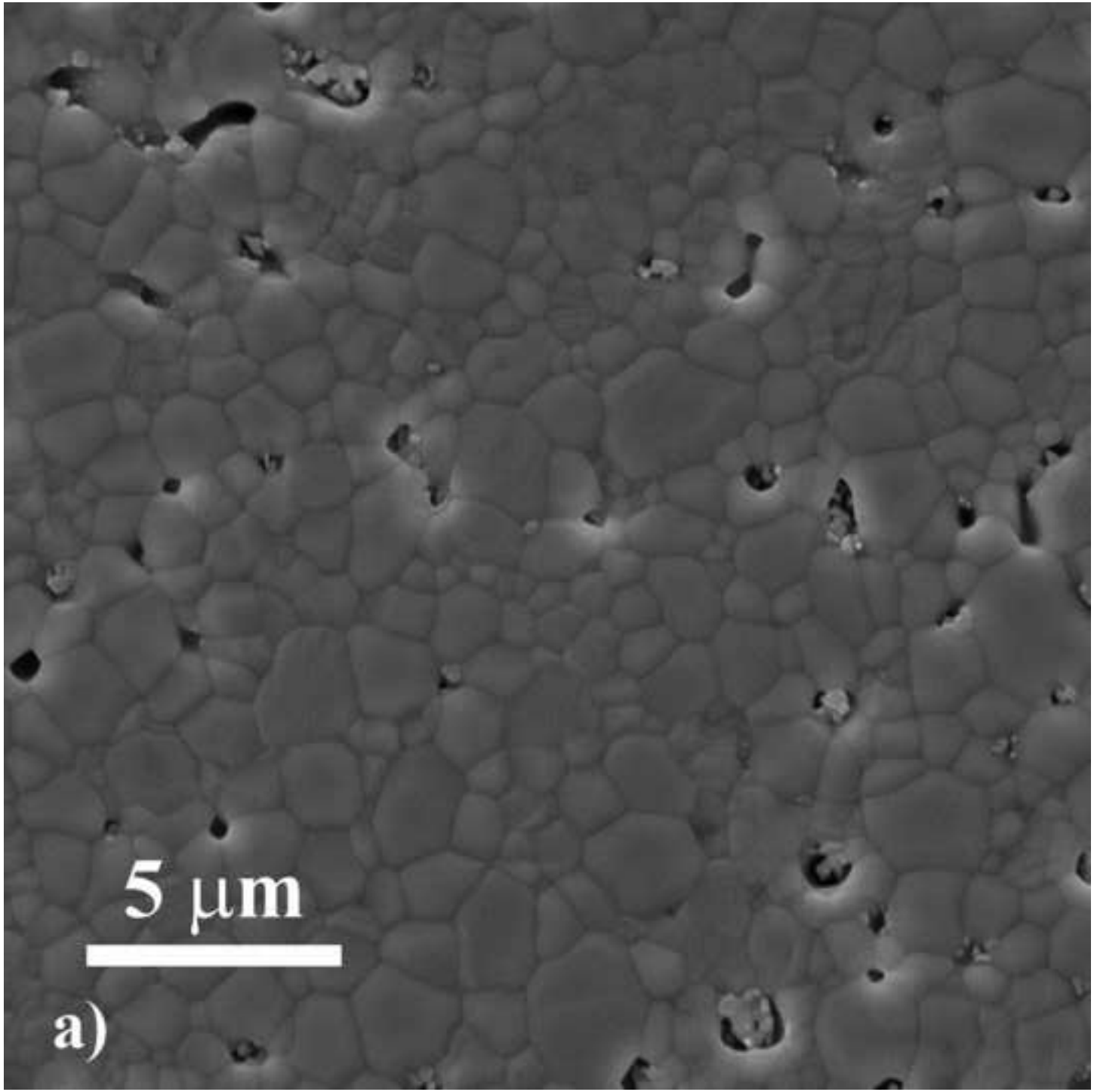

Figure 8b

Click here to download high resolution image

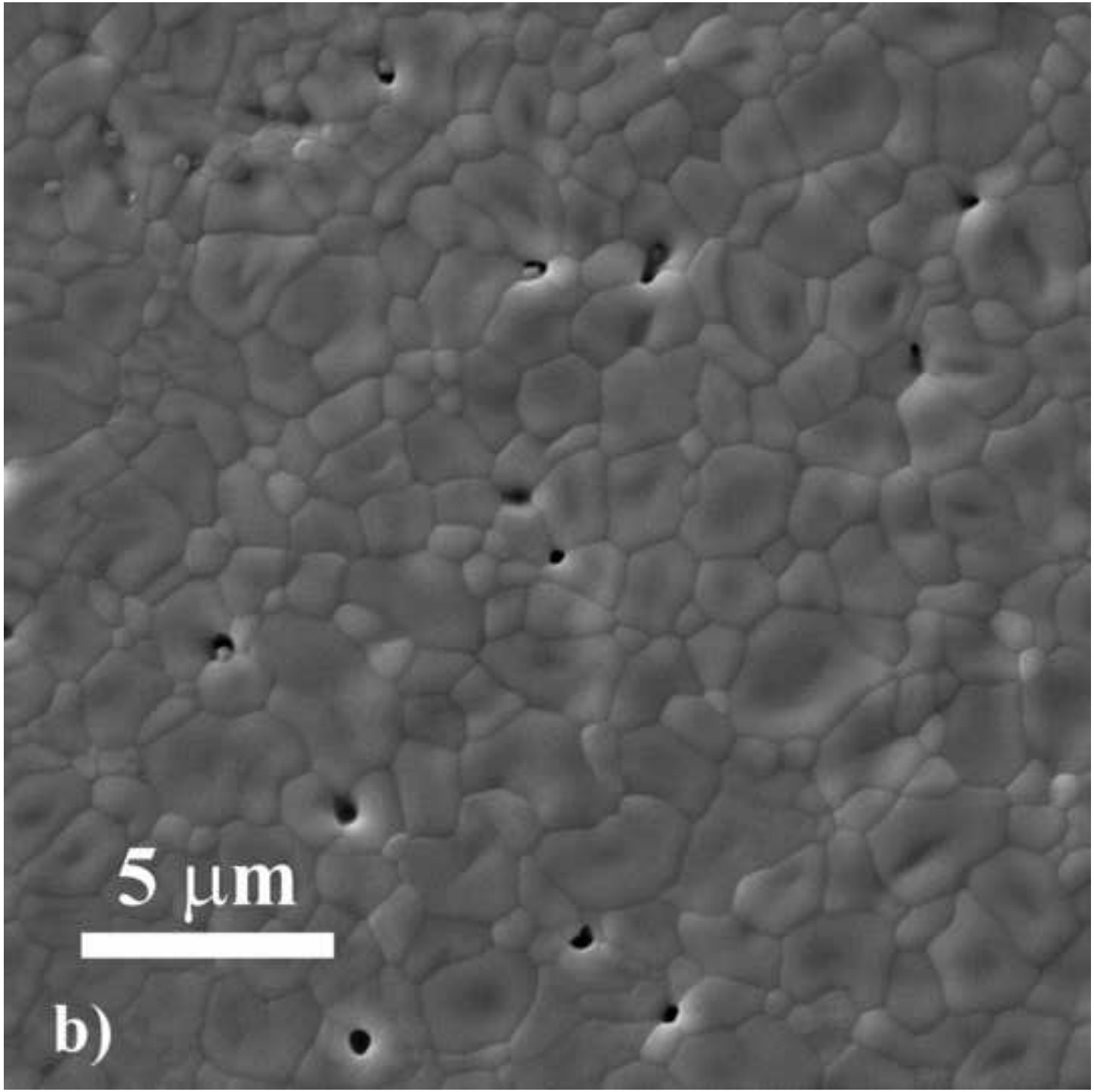

Figure 8c
Click here to download high resolution image

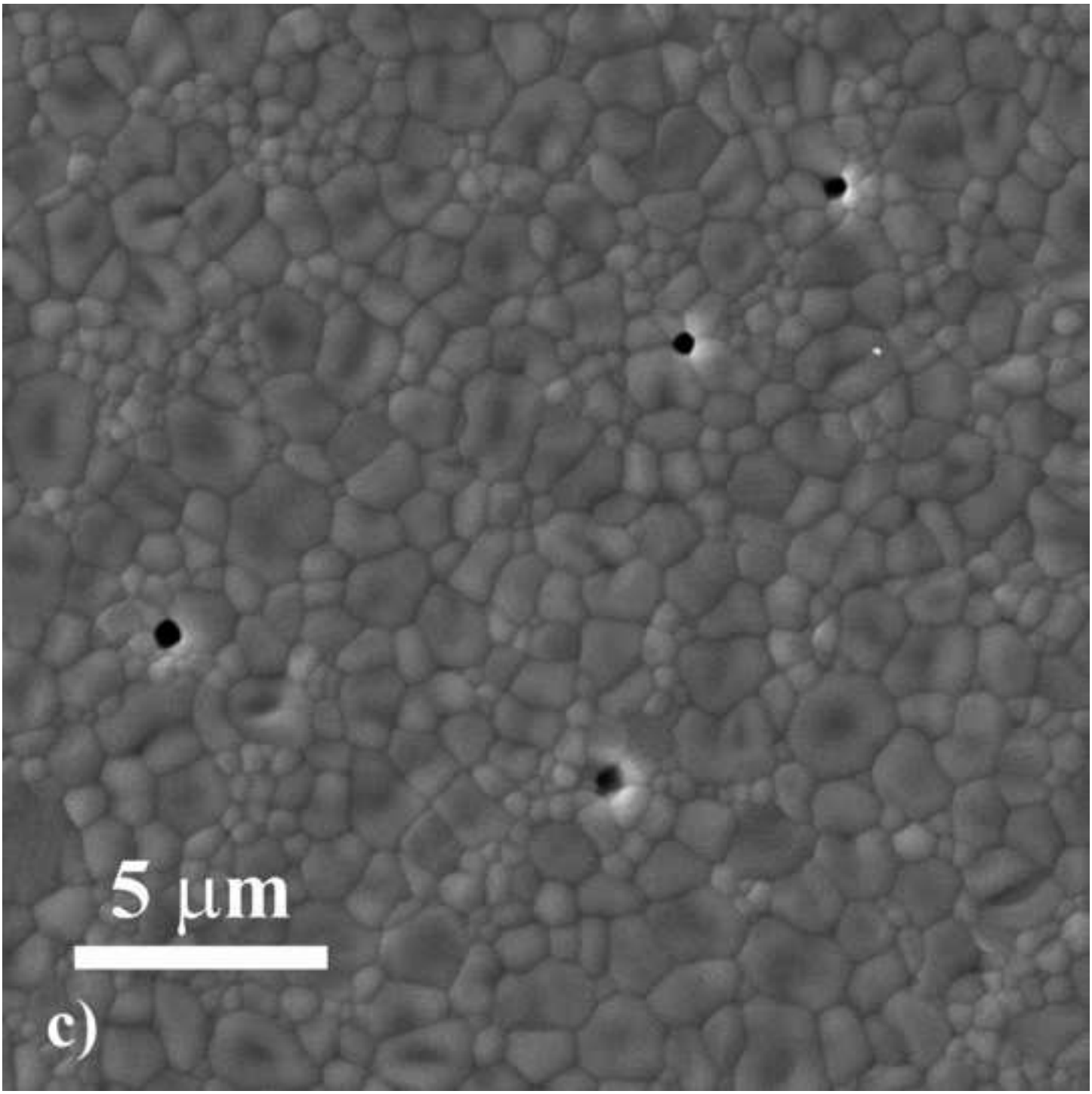

Figure 9

Click here to download high resolution image

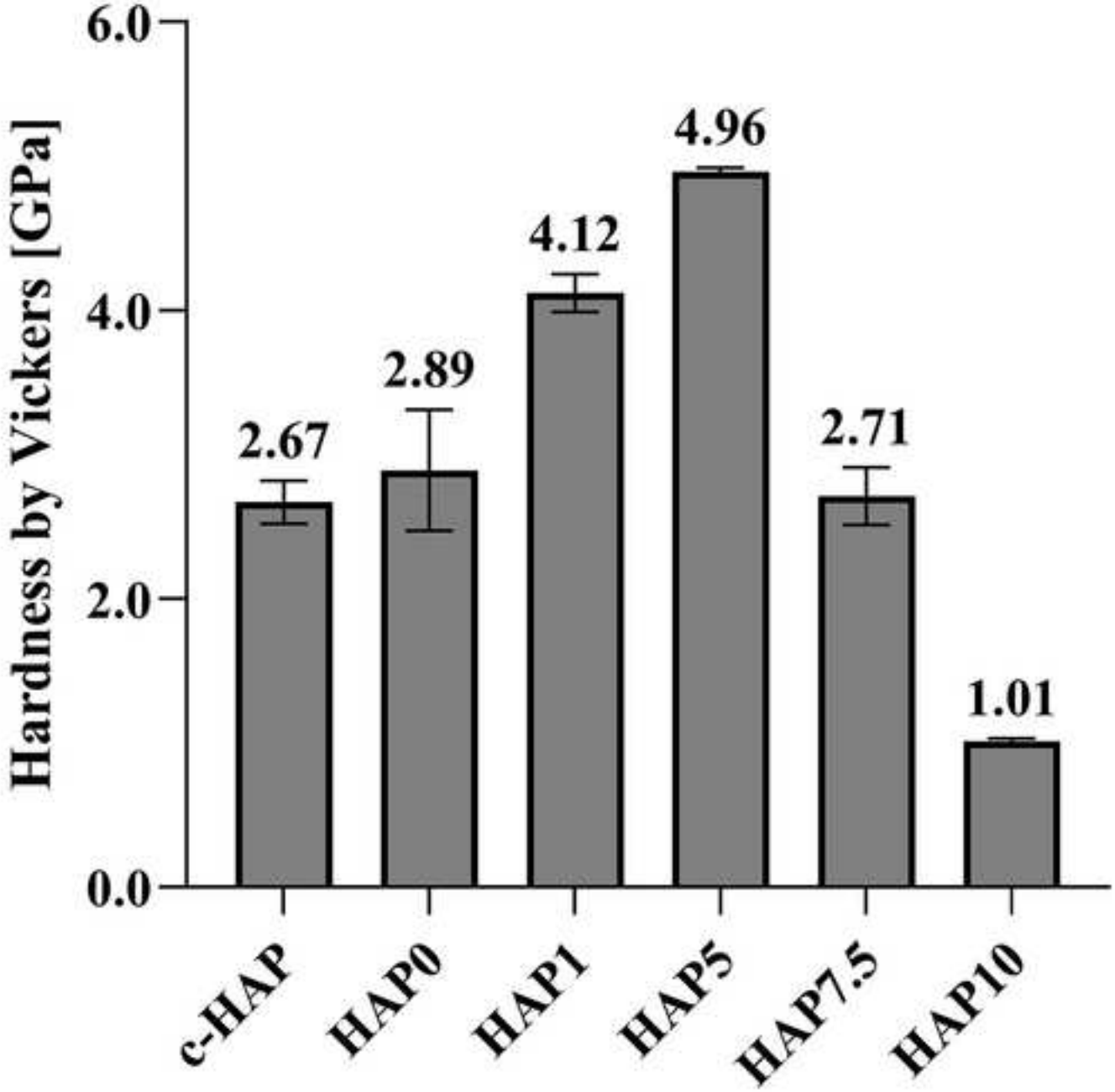

Figure 10
Click here to download high resolution image